The Astrophysical Journal Supplement Series, 173:619–642, 2007 December

UV-OPTICAL COLORS AS PROBES OF EARLY-TYPE GALAXY EVOLUTION

S. Kaviraj,[1] K. Schawinski,[1] J. E. G. Devriendt,[1,2] I. Ferreras,[1,3] S. Khochfar,[1] S.-J. Yoon,[1,4] S. K. Yi,[1,4] J.-M. Deharveng,[5] A. Boselli,[5] T. Barlow,[6] T. Conrow,[6] K. Forster,[6] P. G. Friedman,[6] D. C. Martin,[6] P. Morrissey,[6] S. Neff,[7] D. Schiminovich,[8] M. Seibert,[6] T. Small,[6] T. Wyder,[6] L. Bianchi,[9] J. Donas,[5] T. Heckman,[9] Y.-W. Lee,[4] B. Madore,[10] B. Milliard,[5] R. M. Rich,[11] and A. Szalay[9]

Received 2006 January 4; accepted 2006 September 11

ABSTRACT

We have studied ~2100 early-type galaxies in the SDSS DR3 which have been detected by the *GALEX* Medium Imaging Survey (MIS), in the redshift range $0 < z < 0.11$. Combining *GALEX* UV photometry with corollary optical data from the SDSS, we find that, at a 95% confidence level, *at least* ~30% of galaxies in this sample have UV to optical colors consistent with *some* recent star formation within the last Gyr. In particular, galaxies with an NUV $- r$ color less than 5.5 are *very* likely to have experienced such recent star formation, taking into account the possibility of a contribution to NUV flux from the UV upturn phenomenon. We find quantitative agreement between the observations and the predictions of a semianalytical ΛCDM hierarchical merger model and deduce that early-type galaxies in the redshift range $0 < z < 0.11$ have ~1%–3% of their stellar mass in stars less than 1 Gyr old. The average age of this recently formed population is ~300–500 Myr. We also find that "monolithically" evolving galaxies, where recent star formation can be driven *solely* by recycled gas from stellar mass loss, *cannot* exhibit the blue colors (NUV $- r < 5.5$) seen in a significant fraction (~30%) of our observed sample.

Subject headings: galaxies: elliptical and lenticular, cD — galaxies: evolution — galaxies: formation — galaxies: fundamental parameters

1. INTRODUCTION

One of the most important unresolved debates in contemporary astrophysics concerns the formation mechanism of early-type galaxies. In the classical "monolithic" model (e.g., Larson 1974; Chiosi & Carraro 2002), early-type stellar populations form in a single, short, highly efficient burst of star formation at high redshift ($z \gg 1$), which is followed by passive aging to present day. Such a scenario can explain many of the observed properties of early-type galaxies, both at local and high redshift (Chiosi & Carraro 2002), without invoking hierarchical merger-driven processes (e.g., Toomre & Toomre 1972; Toomre 1977; Kauffmann et al. 1993; Somerville & Primack 1999; Benson et al. 2000; Cole et al. 2000; Hatton et al. 2003, hereafter H03; Khochfar & Burkert 2003). Observational evidence that might *conclusively* rule out either the monolithic or the merger-based scenario has remained elusive (see Peebles 2002 for a critical review of the two paradigms).

The properties of optical color-magnitude relations (CMRs) of early-type galaxies have often been taken as evidence in favor of the monolithic scenario. The lack of redshift evolution of the slope and scatter in optical CMRs (e.g., Bower et al. 1992, 1998; Ellis et al. 1997; Stanford et al. 1998; Gladders et al. 1998; van Dokkum et al. 2000) is consistent with a high formation redshift ($z > 2$), as is the evolution in their zero point. However, the predicted star formation histories (SFHs) of early-type galaxies in the merger paradigm make such a conclusion far less clear cut. For example, the predicted SFHs of (cluster) early-types in the merger scenario are *quasi-monolithic*, with an *overwhelming* majority of the stellar mass forming before a redshift of 1 (Kaviraj et al. 2005a). A careful treatment in the merger framework suggests that the observed optical CMR can *also* be reconciled comfortably with merger models. From a photometric point of view, optical colors are, at best, *degenerate* with respect to the competing theories of early-type galaxy formation, and it is very difficult to discriminate between them using optical colors alone (Kaviraj et al. 2005a).

Evidence does exist for morphological evolution in galaxies, suggesting that formation mechanisms of early-types are *at least not uniquely monolithic*. Although approximately 80% of galaxies in the cores of present day clusters have early-type morphologies (Dressler 1980), a higher fraction of spiral galaxies have been reported in clusters at $0.3 < z < 0.8$ (e.g., Butcher & Oemler 1984; Dressler et al. 1997; Couch et al. 1998; van Dokkum et al. 2000), along with increased rates of merger and interaction events (e.g., Couch et al. 1998; van Dokkum et al. 1999). This is supported by recent results which suggest that the mass density on the red sequence (which is dominated by early-type systems) has doubled since $z = 1$ (Bell et al. 2004). The strengths of age-sensitive spectral indices observed in some early-type systems require luminosity-weighted ages that are consistent with the presence of at least some recent star formation (RSF) in these systems (e.g., Caldwell et al. 2003; Trager et al. 2000a, 2000b; Proctor & Sansom 2002).

Furthermore, some nearby early-type galaxies exhibit unambiguous signs of significant ongoing or recent star formation, such as NGC 5128 (e.g., Rejkuba et al. 2001; Peng et al. 2004; Yi et al. 2004; Kaviraj et al. 2005b; Rejkuba et al. 2004), NGC 205 (Hodge

[1] Department of Physics, University of Oxford, Oxford OX1 3RH, UK.
[2] Observatoire Astronomique de Lyon, 9 Avenue Charles André, 69561 Saint-Genis-Laval Cedex, France.
[3] Department of Physics, King's College London, Strand, London WC 2R 2LS, UK.
[4] Center for Space Astrophysics, Yonsei University, Seoul 120-749, Korea; yi@yonsei.ac.kr.
[5] Laboratoire d'Astrophysique de Marseille, 13376 Marseille Cedex 12, France.
[6] California Institute of Technology, MC 405-47, Pasadena, CA 91125.
[7] Laboratory for Astronomy and Solar Physics, NASA Goddard Space Flight Center, Greenbelt, MD 20771.
[8] Department of Astronomy, Columbia University, MC 5246, New York, NY 10027.
[9] Department of Physics and Astronomy, Johns Hopkins University, Baltimore, MD 21218.
[10] IPAC, 770 South Wilson Avenue, Pasadena, CA 91125.
[11] Department of Physics and Astronomy, University of California, Los Angeles, CA 90095-1562.

1973; Burstein et al. 1988), NGC 5102 (Pritchet 1979; Burstein et al. 1988; Deharveng et al. 1997), and certain early-type systems recently mapped by the SDSS (Fukugita et al. 2004).

Others, such as NGC 2865 (Bica & Alloin 1987), NGC 5128 (Schiminovich et al. 1994), and NGC 3921 (Schweizer et al. 1996), provide direct residual evidence of the recent interactions that created them (see also papers by the SAURON collaboration, e.g., Falcon-Barroso et al. [2006] and references therein).

It is worth noting that, contrary to the traditional notion that early-type galaxies are largely devoid of cold gas, observational evidence over the last 30 years (e.g., from *IRAS*) has shown that this is *not* the case.

Cold gas, which supplies the fuel for star formation, has been detected in significant numbers of nearby early-type systems (e.g., Knapp et al. 1989; Knapp & Rupen 1996; Young 2005, also see the review by Knapp 1999). Thus, it is perhaps correct to *expect* RSF in early-type galaxies, rather than consider them inert, passively evolving systems.

Given the apparently evolving early-type fraction and accumulating spectrophotometric evidence for RSF in nearby early-type galaxies, it is vital to establish whether RSF may only be a sporadic feature of a few early types or a more widespread phenomenon in the early-type population. The confirmation of low-level star formation *in a significantly large sample of low-redshift early-type galaxies* would put powerful constraints on models for their formation.

Spectroscopic indicators of RSF are already available, such as the commonly used Hβ index, higher order Balmer lines such as Hγ and Hδ, and the D4000 break. From a photometric point of view, rest-frame ultraviolet flux is highly sensitive to RSF. Given the apparent degeneracy in optical colors, ultraviolet photometry offers the best route to finding tell-tale signatures of RSF in early-type systems at low redshift, if indeed such star formation is present in these systems.

In a recent work, Ferreras & Silk (2000b, hereafter FS00) studied a sample of early-type galaxies in the cluster Abell 851 at $z = 0.41$. They used F300W (rest-frame near-ultraviolet [NUV], 2300 Å) and optical photometry to perform one of the first studies of the NUV -optical CMR in a sample of early-type galaxies. They found that the slope and scatter of the NUV-optical CMR was consistent with some early-types having $\sim$10% of their stellar mass in stars younger than $\sim$500 Myr. Detailed modeling of this data (Ferreras et al. 2002) indicated that secondary bursts of star formation at low redshifts lead to a natural explanation of the large scatter in the NUV-optical CMR.

More recently, Deharveng et al. (2002) studied the rest-frame flux around 2000 Å from a sample of 82 nearby early types using data from the FOCA, SCAP, and FAUST experiments. The focus of this study was primarily to investigate the far-ultraviolet (FUV) emission of early-type galaxies, thought to originate from old extreme horizontal branch (EHB) stars and their progeny (Yi et al. 1997). Note, however, that the filter used in this study is centered between the typical FUV peak wavelength of 1500 Å and the NUV peak of 2300 Å. Their analysis suggested that the $2000 - V$ colors in some early-type galaxies are significantly bluer than would be expected from old populations alone and cannot be explained without invoking some RSF.

Low-redshift photometry in the far-ultraviolet (FUV; 1530 Å) and near-ultraviolet (NUV; 2310 Å) passbands from the *GALEX* mission (Martin et al. 2005), unprecedented both in terms of its quality and quantity, provides a unique opportunity to study the RSF-sensitive UV emission from a variety of nearby early-type galaxies across a range of luminosities and environments. In this paper we study $\sim$2100 early-type galaxies detected by *GALEX*, in the redshift range $0 < z < 0.11$. We focus mainly on the NUV passband, because the FUV is sensitive not only to RSF but also to the UV upturn flux from EHB stars that could be expected in old early-type populations. The NUV is less sensitive to UV upturn and therefore a better RSF indicator.

A preliminary study of the UV emission of early-types, based on *GALEX* detections of SDSS early-type galaxies listed in the catalog of Bernardi et al. (2003d, hereafter B03) was presented in Yi et al. (2005). Comparing the photometry of early-types in this sample to the spectral energy distribution (SED) of a strong nearby UV -upturn galaxy (NGC 4552), they did not find more than 2 galaxies (out of 162) that fit the typical UV-optical shape of a system with a significant amount of UV upturn flux. They concluded that the large scatter in the NUV $- r$ colors cannot be generated from a scatter in late-stage stellar evolution alone. We also direct readers to Boselli et al. (2005), who were the first to perform a detailed study of the UV CMR in the Virgo cluster. However, we note that our sample covers a wide variety of environments and we sample almost 2 mag deeper (in r band) in dense environments (see Schawinski et al. 2007) compared to the Virgo sample of Boselli et al. (2005).

We begin this study by describing the construction of an early-type catalog, similar to that used in Yi et al. (2005) but in which the morphological classification of objects and removal of potentially UV-contaminating AGNs are performed in a more robust manner. Using a simple parameterization of the SFH, we identify galaxies that appear to have had *some* star formation within the last Gyr. We use a semianalytical ΛCDM model, calibrated to accurately reproduce the (cluster) optical CMR in the redshift range $0 < z < 1.27$ (see Kaviraj et al. 2005a), to predict the NUV CMR and compare it to observations. Finally, we discuss the comparative roles of quiescent and merger-driven processes in driving the residual star formation found in some of our early-type sample and investigate whether an *extreme* monolithic scenario is capable of reproducing the NUV colors of large ($>L_*$), blue (NUV $-$ $r < 5.5$) early-type galaxies in our sample.

2. SAMPLE SELECTION

2.1. *Constructing an Early-Type Catalog from the SDSS DR3*

B03 were the first to construct an SDSS catalog of $\sim$9000 early-type galaxies, selected using a combination of SDSS pipeline parameters (see also Bernardi et al. 2003a, 2003b, 2003c, 2003d for a comprehensive study of the properties of galaxies in this catalog). Their catalog contains galaxies with high i-band concentration indices ($r_{50}/r_{90} > 2.5$), spectral classifications typical of early-type galaxies, and where the de Vaucouleurs fit to the surface brightness profile is more likely than the exponential fit. While such automated prescriptions are very efficient at selecting a reasonably robust early-type galaxy sample, it suffers from two shortcomings.

First, it is apparent from visually inspecting a sample of Bernardi early types that it contains late-type contaminants, such as sideways-on spirals, Sa-type galaxies, and objects where a central dominant bulge is surrounded by faint spiral features. While clearly not early-type galaxies, these objects all pass the selection criteria. The UV emission from early-type galaxies is predicted to be weak in any galaxy formation scenario. The presence of late-type contaminants is therefore a particular problem, since such galaxies will be substantially bluer than true early types and our conclusions regarding the presence of star formation in the early-type population could be severely affected.[12]

[12] We must note, however, that given the size of the B03 sample, performing a visual inspection of *all* galaxies is clearly impractical.

Second, *spectral* selection criteria, such as those used in B03, immediately exclude any early-type galaxy that may contain star formation and therefore spectral lines, such as those reported by Fukugita et al. (2004). Since one of our main aims is to test galaxy formation models and attempt to discriminate between the monolithic and merger driven paradigms, we must take special care not to bias our sample toward one scenario at the outset. Clearly, removing early-type systems with signs of star formation will bias the sample toward the passive monolithic models and make any conclusions regarding the recent star formation activity in early-types less meaningful.

Since robust morphological classification inevitably requires visual confirmation of early-type candidates, our approach to constructing an early-type catalog relies more on visual inspection of each candidate than automatic extraction based on pipeline parameters. We make our initial selection of objects based on a single SDSS parameter, fracDev, which is the weight of the de Vaucouleurs fit in the best composite (de Vaucouleurs + exponential) fit to the galaxy's image in a particular band. We extract all galaxies that have fracDev > 0.95 in g, r, and i bands. The short-wavelength g-band traces disk or spiral arm structures, while r and i trace the central bulge. The robustness of this procedure has been checked by applying it to a sample of 200 randomly selected nearby early-type galaxies from the SDSS DR3. We find that 90% of the early-types in this sample (confirmed by visual inspection) have fracDev > 0.95. This implies that, on average, this criterion would pick up 90% of the galaxies in a typical sample of SDSS galaxies. Reducing the value of fracDev $= 0.95$ would admit more early types but also increase contamination, resulting in a larger sample of galaxies to be processed visually. A fracDev value of 0.95 gives the best trade-off between selecting a sample dominated by early-type objects and a sample with a significant amount of contamination. Note that we have chosen not to make a distinction between elliptical and S0 galaxies in this study since it is difficult to discriminate between them effectively using the SDSS images. It is worth noting, however, that these two populations could behave differently (e.g., Boselli et al. 2005).

Having extracted our initial working sample of galaxies, we perform a visual inspection of each early-type candidate. However, our sample of galaxies spans a large range in luminosity and redshift. Our ability to accurately classify any galaxy depends on the clarity of its features on the SDSS image; this in turn depends on its redshift and apparent luminosity. Thus, we must first determine the *limiting* redshift and luminosity at which we can *trust* our classifications.

The average SDSS exposure time is 50 s. To perform this check we use 24,000 s exposure COMBO-17 images of SDSS galaxies, at redshifts between 0.11 and 0.13 (kindly provided by Chris Wolf). The high exposure time of the COMBO-17 images allows us to resolve all features within the galaxies in question. We find that, for an apparent r-band magnitude of 16.8, our classification based on the SDSS images matches that based on the COMBO-17 images. We therefore apply a redshift cut of 0.11 and an apparent r-band magnitude cut of 16.8 to our sample, to extract a magnitude limited sample of $\sim$3500 SDSS early-type galaxies (see Schawinski et al. 2007 for more details).

2.2. *Cross-Matching with GALEX MIS Detections*

We direct readers to Martin et al. (2005) and Morrissey et al. (2005) for a description of the scope and performance of the *GALEX* satellite. The magnitude-limited SDSS early-type sample described in § 2.1 is now cross-matched with data from 595 *GALEX* fields, imaged in the medium depth (MIS) mode. *GALEX* has a fiducial angular resolution of 6″. The positional matching is performed within a more conservative 4″. We eliminate any *GALEX* objects that have multiple SDSS matches within 6″ because it is impossible to tell which companion dominates the UV flux detected by *GALEX*. We find that the fraction of galaxies in our magnitude limited sample ($r < 16.8$, $z < 0.11$) detected by *GALEX* is around 90%–95% (Fig. 1). The detection rate drops sharply after $z = 0.11$.

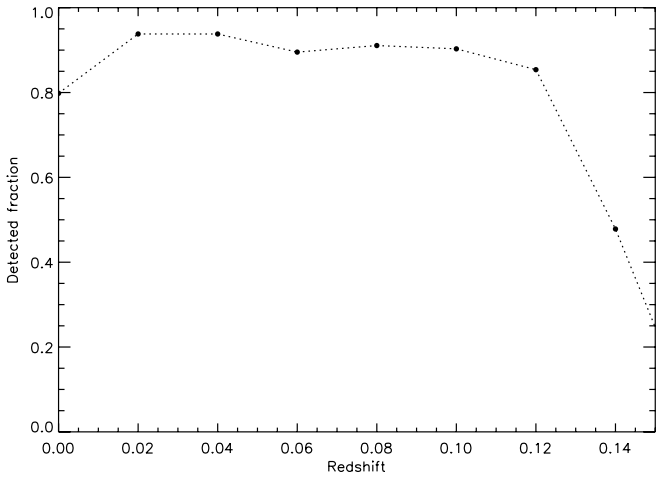

FIG. 1.—Fraction of SDSS early types in MIS fields that are detected by *GALEX*.

2.3. *AGN Diagnostics: Optical Analysis*

Since we are studying the (generally weak) rest-frame UV flux from early-type galaxies here, it is important to ascertain the level of possible contamination of the UV continuum due to nonthermal emission from AGNs, which are common in early-type galaxies. Rich et al. (2005), who employed a similar method to B03 to extract a sample of early-type galaxies from the SDSS and study their UV emission detected by *GALEX*, were the first to perform this additional check for AGN contamination, using emission lines measured by the SDSS. Following their study, we perform a similar analysis to gauge the contribution from AGNs to the rest-frame UV in our galaxies, and eventually remove those that exhibit signs of hosting a strong AGN.

Type I (i.e., unobscured) AGNs are largely removed by using the SDSS spectral classification algorithm (by setting the QSO flag) during our initial extraction of galaxies. Any remaining type Is are then removed completely through the optical and radio analyses we describe below. Type II (i.e., partly obscured) AGNs can be distinguished from normal (star-forming) galaxies using the intensity ratios of pairs of strong emission lines (Baldwin et al. 1981, hereafter BPT81). Using the emission line ratios [O III/Hβ] and [N II/Hα], Kauffmann et al. (2003, hereafter K03) have used a BPT81-type analysis to classify a large sample of SDSS galaxies into star-forming and type II AGNs (Seyferts, LINERs, and transition objects). We identify and remove potential AGNs from our sample using the criteria derived by K03.

Before calculating line ratios, we must correct for possible absorption in these line regions and extract the true emission strengths of each line index. We first construct a library of 10,000 star formation histories (SFHs) in which each SFH is modeled by an instantaneous starburst at $z = 3$ followed by a second instantaneous starburst, which is allowed to vary in age and mass fraction. The choice of this model library is motivated by the fact that our galaxy sample contains *only* early-type objects, and we find

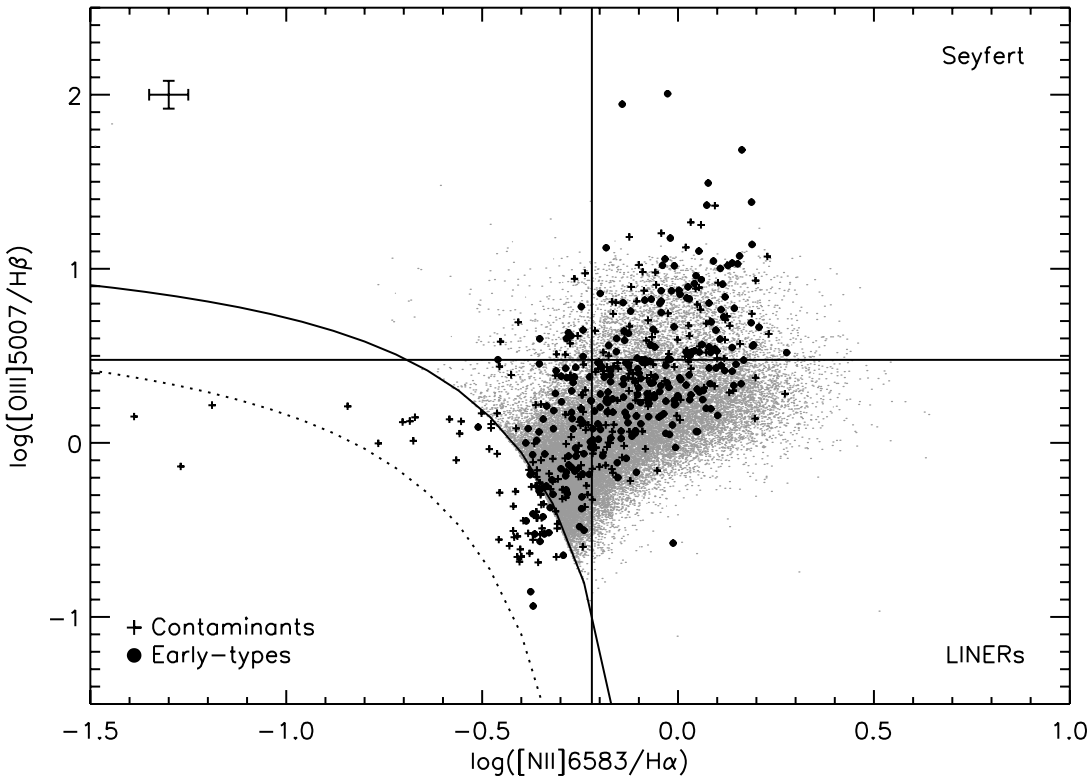

FIG. 2.—Plot of [O III/Hβ] vs. [N II/Hα] used to find and remove AGNs in our sample. The curved line represents the demarcation between star-forming systems and type II AGNs. Galaxies are considered star-forming if they lie below this line. Large dots represent galaxies identified as early-type after visual inspection. Crosses represent galaxies identified as contaminants in our initial sample of galaxies. The small gray dots are K03's SDSS type II AGN catalog. It is worth noting that the star-forming locus (enclosed by the solid curve and the bold dotted line) is almost completely empty, which is expected since our sample is composed exclusively of early-type galaxies. In addition, the majority of galaxies that lie on the star-forming locus are contaminants.

that such model SFHs give excellent fits to the stellar continua of galaxies in our sample. While studies such as K03 have to deal with the full spectrum of morphological types and thus require more elaborate model libraries, we tailor our model library to the narrow set of morphologies spanned by our sample. The stellar models used to compute the model library in Yi et al. (1997) and Yi (2003) adopt the universal Salpeter IMF.

The procedure for correcting for absorption proceeds in the standard way, by first comparing the spectrum of each observed galaxy (excluding major line emission regions) to the model library and finding the best-fit model. The absorption strengths of the O III, Hβ, N II, and Hα lines in the best-fit model are then computed and subtracted from the measured line strengths in the observed spectrum. For each galaxy that exhibits all four emission lines with a signal-to-noise ratio (S/N) greater than 3, we construct the line ratios, place the galaxy on a plot of [O III/Hβ] versus [N II/Hα], and classify it as either star-forming or a type II AGN, based on the criteria derived by K03.

In Figure 2 we plot [O III/Hβ] versus [N II/Hα] used to find and remove AGNs in our sample. The curved line represents the demarcation between star-forming systems and type II AGNs. Galaxies are considered star-forming if they lie below this line. Filled circles represent galaxies identified as early-type after visual inspection. Crosses represent galaxies identified as contaminants in our initial sample of galaxies. The small gray dots are K03's SDSS type II AGN catalog. It is worth noting that the star-forming locus (see Fig. 1 in K03 for comparison) is almost completely empty, which is expected since our sample is composed exclusively of early-type galaxies. In addition, the majority of galaxies that do lie on the star-forming locus are contaminants. This optical analysis identifies $\sim$25% of our early-type sample as type II AGNs.

2.4. *AGN Diagnostics: Radio Analysis*

Galaxies that either do not have the four required emission lines, or in which emission line detections have S/N < 3, cannot be treated using the optical analysis discussed above. In most studies these galaxies are assumed to have no contribution from AGNs. However, we opt not to make this assumption and confirm the results of the optical analysis for galaxies that remain unclassified using their radio emission. There are two radio surveys that overlap with our early-type sample: the FIRST survey (Becker et al. 1995), which has an angular resolution of $\sim$5″ and a completeness limit of 1 mJy, and the NVSS survey, which has an angular resolution of 45″ and a completeness limit of 2.5 mJy.

In this study we use the FIRST survey due to its superior resolution and depth—we find that including NVSS in our analysis does not add to or alter our conclusions. The high resolution of FIRST poses a slight problem for sources for which the radio emission is not very centralized. For example, galaxies with radio lobes have multiple, spatially resolved detections in FIRST. We therefore cross-match our early-type sample with FIRST detections using a large search radius of 30″. If there are multiple detections within this search radius we add the fluxes of all the detections corresponding to the early-type object in question.

To identify a luminosity threshold above which radio activity could be attributed to AGNs, we compare the radio luminosities of galaxies classified by the previous optical analysis as normal (i.e., star-forming) to the luminosities of those classified as type II AGNs. We show this comparison in Figure 3. Plus signs show normal (star-forming) galaxies, while other symbols correspond to various classes of type II AGNs. We find that type II AGNs tend to dominate this plot above a radio luminosity of $\sim 10^{22}$ W Hz^{-1},

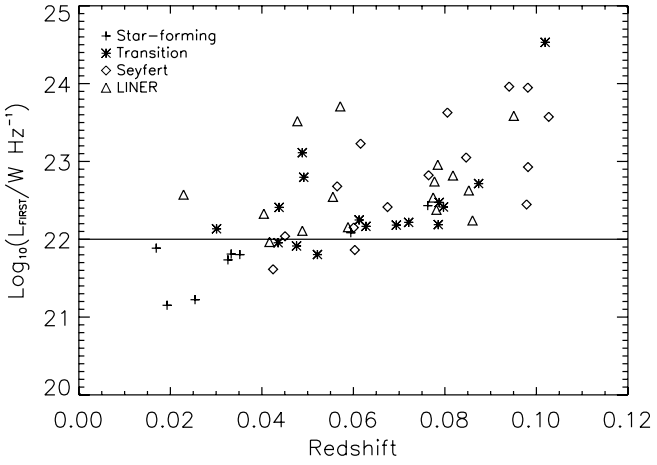

FIG. 3.—Comparison of radio luminosities of galaxies classified by the optical analysis as normal (*crosses*) and type II AGNs (*all other symbols*; see legend for specific AGN classifications). Type II AGNs tend to dominate this plot above a radio luminosity of $\sim 10^{22}$ W Hz^{-1}, while most of the normal (i.e., star-forming) objects lie below this threshold.

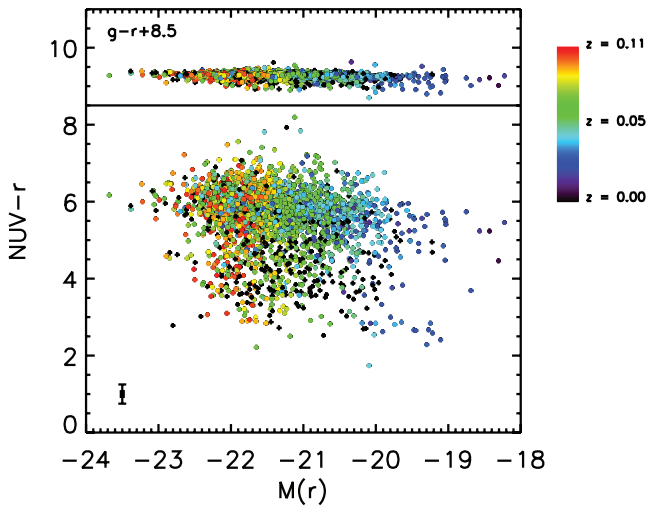

FIG. 4.—Optical (*top*) and the NUV $-$ r (*bottom*) color-magnitude relations (CMRs) of our early-type galaxies. We intentionally show the optical CMR on the same scale as its UV counterpart, to highlight the significant difference in their respective scatters. Galaxies are color-coded according to their redshifts. The small gray crosses represent galaxies that are rejected based on the optical or radio analyses.

while most of the normal (i.e., star-forming) objects lie below this threshold. We use this threshold and remove any galaxy that remains unclassified in the optical analysis but shows a radio luminosity above 10^{22} W Hz^{-1}. This removes $\sim$3% of the sample of galaxies that survive the optical analysis.

We must note, however, that galaxies with a high radio luminosity do not necessarily host AGNs. There is a degeneracy between radio emission from AGNs and from genuine star formation, which is not quantified accurately by using a single threshold value. By applying this cut we might indeed exclude interesting early-type galaxies that are genuinely star-forming. However, since the radio analysis only affects a small fraction of our sample, we *include* it in our sample selection, as it would only make our sample slightly more conservative in terms of star-forming early-type galaxies.

2.5. *The Final Catalog*

Table 1 summarizes all the criteria used in the construction of our final catalog of early-type galaxies. The final sample contains 2116 galaxies.

Figure 4 shows the optical (*top*) and the NUV $-$ r (*bottom*) color-magnitude relations (CMRs) of our early-type galaxies. Galaxies are color-coded according to their redshifts. The small gray crosses represent galaxies that are rejected based on the optical or radio analyses described in the previous sections. At first glance, the tight optical CMR typical of early-type populations is in stark contrast to the large spread in colors evident in the NUV CMR. While the scatter in the optical CMR is approximately 0.05 mag, the spread in the NUV colors is almost 6 mag with a (biweight) scatter of approximately 1 mag. The properties of the NUV CMR immediately lead to two conclusions.

First, it seems inconsistent with a monolithic evolution scenario for all galaxies in our sample. If all early types were dustless simple stellar populations (as is frequently assumed from their tight optical CMRs in the context of the monolithic picture), we might expect the NUV CMR to be *just as tight* as its optical counterparts. In reality, any age dispersion, coupled with the presence of varying amounts of UV upturn, might be expected to induce some scatter in the NUV CMR. A lower limit to the NUV $-$ r color in such a hypothetical monolithic CMR can be estimated by looking at the NUV $-$ r color of the nearby strong UV-upturn galaxy, NGC 4552. We use a composite spectrum of NGC 4552, in which the UV spectral ranges are constructed from *IUE* and *HUT* data (see caption of Fig. 1 in Yi et al. [1998] for more details on sources in the construction of this composite SED), to estimate this lower limit. This composite SED yields an NUV $-$ r color of 5.4. We should note, however, that the UV component, derived from *IUE* and *HUT* data, samples the UV bright core of NGC 4552, so the value of 5.4 is likely to be *bluer* than the NUV $-$ r color averaged over the entire galaxy. This makes NUV $-$ $r = 5.4$ an optimistic estimate for the blue end of a monolithic CMR. However, in a monolithic scenario all the galaxies would have NUV $-$ $r \geq 5.4$, which is clearly not the case for the galaxies in our sample. We can therefore assume that the excess scatter in the NUV CMR is due, at least in part, to some recent star formation.

Second, it is apparent that the *red envelope* is not very well-defined; i.e., we do not see a sharp red edge to the NUV CMR as is frequently seen in optical CMRs. This is likely to be caused by varying levels of dust (and therefore gas) in these galaxies that *smear out* the tightness in the red sequence.

TABLE 1

SUMMARY OF CRITERIA USED IN CONSTRUCTING THE SDSS-*GALEX* EARLY-TYPE CATALOG

Criterion	Reason
$r < 16.8$	Robust morphology (from COMBO-17 comparison)
$z < 0.11$	Robust morphology, *GALEX* detection rate stable at 90%
Emission line analysis	AGN removal for emission line galaxies with S/N > 3
L(radio) > 10^{22} W Hz^{-1}	Further removal of possible AGNs not classified by the emission line analysis

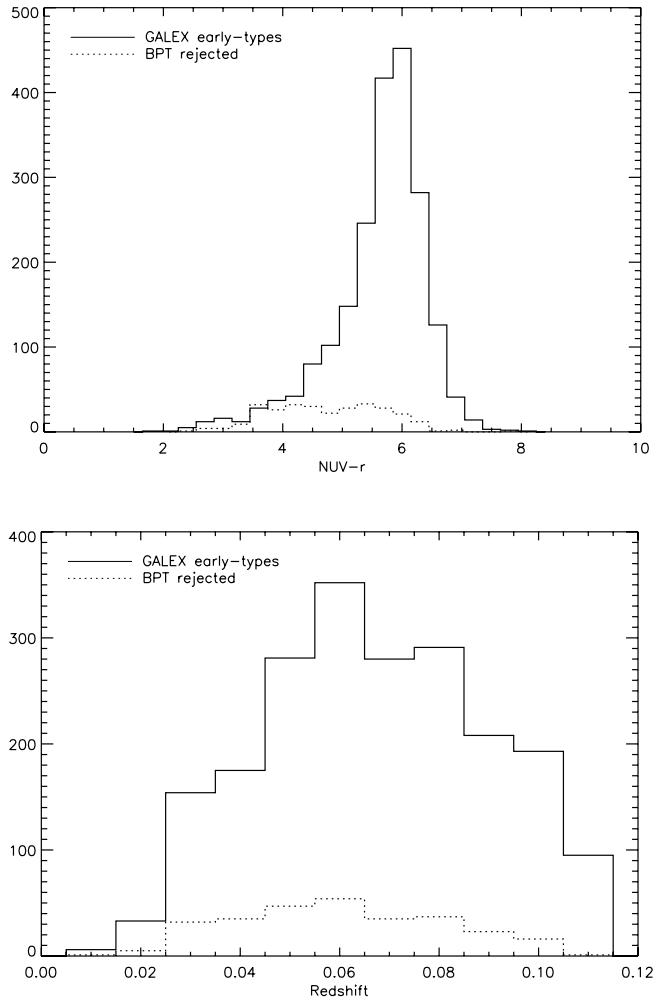

FIG. 5.—Comparison of BPT81 rejected galaxies to galaxies in our final catalog. The BPT81 rejected galaxies prefer bluer NUV − *r* colors, which is not unexpected since the AGN contribution to the continuum would be expected to make the NUV color bluer. There appears to be no bias with redshift—we do not expect the fraction of AGNs hosting galaxies to change significantly over this redshift range.

Note that NUV colors are a factor of 4 more sensitive to dust than optical colors such as $(g - r)$, so the presence of a small amount of dust can have a proportionately larger effect in the NUV than in the optical spectral ranges.

In Figure 5 we compare the BPT81 rejected galaxies to galaxies in our final catalog. The BPT81 rejected galaxies prefer bluer NUV − *r* colors, which is not unexpected since the continuum AGN contribution makes the NUV color bluer. There appears to be no bias with redshift, which fits our expectation that the fraction of AGNs hosting galaxies will not change significantly over such a small redshift range. In Figure 6 we show the NUV luminosities of early-types in our sample as a function of redshift. The yellow region shows the detectable $M_{\rm NUV}$ space, assuming the fiducial detection limit of the MIS fields ($m(\rm NUV) = 23$; *dashed curve*). The absolute NUV magnitude of the detected early types and their errors are shown by the blue points. Also shown is the expected absolute NUV magnitude of a passively evolving giant early-type galaxy ($M_V = -23$) that forms at $z = 3$, assuming solar (*solid line*) and twice solar (*dashed line*) metallicities. Since the monolithic evolution shown is for an extremely bright early-type galaxy, detections above this line immediately imply that, for at least some early types, a monolithic SFH is not consistent with their detected NUV flux.

As shown in Figure 1, approximately 10% of the SDSS early-types in the *GALEX* field of view remain undetected. To explore the properties of these undetected galaxies, we construct, for each nondetection, a *synthetic* absolute NUV magnitude, based on the assumption that the galaxy is dustless, has solar metallicity and is formed at $z = 3$. We plot these synthetic magnitudes as red points in Figure 6. The filled red circles correspond to undetected galaxies with $r < 16.8$, and the small red points are nondetections with $r > 16.8$. We find that while some nondetections are close to the detection limit, a significant number of these galaxies *should* be detected, under the assumptions used to construct their synthetic magnitude. However, both a supersolar metallicity and/or a small dust content can be sufficient to push these galaxies below the detection limit. We indicate this, in Figure 6, by showing the predicted deviation of the NUV luminosity from the synthetic magnitude assumptions for a small dust content, e.g., $E(B - V) = 0.1$, and nonsolar metallicities.

3. QUANTIFYING THE RSF IN THE *GALEX* EARLY TYPES

The aim of this section is to *quantify* the RSF in our early-type sample. In particular, we would like to establish how many of our galaxies have photometry consistent with any star formation within the last Gyr, at the 95% confidence level.

Before we begin, it is instructive to consider the scope of the NUV in computing age determinations. Figure 7 shows the intrinsic NUV − *r* color of a simple stellar population (SSP) as a function of age and metallicity (solar: *dotted line*; half-solar: *solid line*; twice-solar: *dashed line*). The evolution in the NUV − *r* color slows considerably after 1–2 Gyr, as the NUV flux from a recent starburst decays significantly in this timescale. The NUV is therefore an effective age indicator for only ∼1 Gyr after the starburst in question. In other words, we can expect the UV (+optical) photometry of our galaxies to be able to distinguish only between galaxies that have had a very recent starburst, within the last 1 Gyr and galaxies that have not. The NUV, however, is blind to any star formation that is much older than 1 Gyr old.

We fit the observed colors of the *GALEX* early types across the UV and optical spectral ranges to colors predicted by a library of model SFHs, in which an initial starburst at high redshift ($z = 3$) is followed by a second starburst, which is allowed to vary in mass fraction and age between $z = 3$ and present day. Both starbursts are assumed to be instantaneous. Each model in the library has two main parameters: $t_{\rm YC}$, the age of the second starburst, in the range 10^{-2} to 15 Gyr and $f_{\rm YC}$, the mass fraction of stars formed in the second starburst, in the range 10^{-4} to 1 (YC stands for young component). We explore models with metallicities $Z/Z_\odot$ in the range 0.5–2.5 and intrinsic $E(B - V)$ values in the range 0–0.15. We use the standard dust prescription given in Calzetti et al. (2000) to compute the reddening for a given value of $E(B - V)$. The stellar population models used to compute the model library in this study (Yi et al. 1997; Yi 2003) adopt the universal Salpeter IMF. For galaxies without FUV detection, we use a four-color (NUV − *r*, $g - r$, $r - i$, and $r - z$) comparison, while for those with FUV detection we use five colors (FUV − *r*, NUV − *r*, $g - r$, $r - i$, and $r - z$). We perform a χ^2 test with the appropriate degrees of freedom by minimizing the sum of the normalized residuals

$$\chi^2 = \sum_n^{4/5} \left(\frac{C_n^{\rm mod} - C_n^{\rm obs}}{\sigma_n} \right)^2, \qquad (1)$$

where $C_n^{\rm mod}$ and $C_n^{\rm obs}$ are the *n*th model and observed colors, respectively, and σ_n is the uncertainty in the residual $C_n^{\rm mod} - C_n^{\rm obs}$.

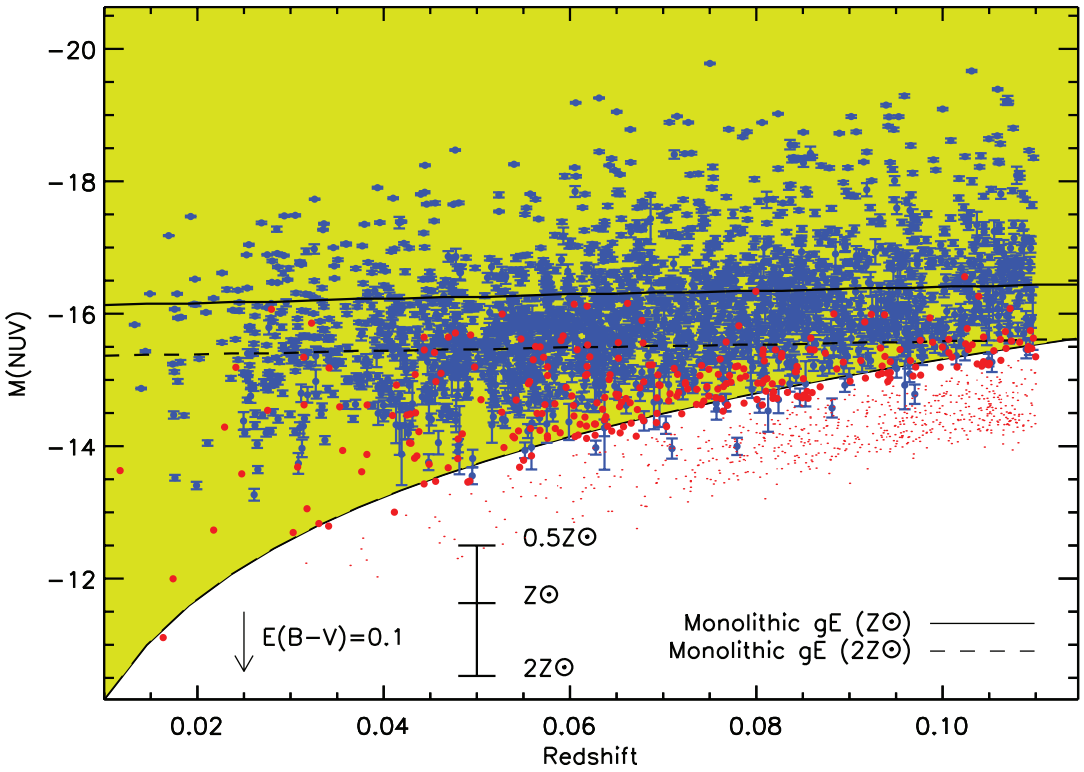

FIG. 6.—SDSS early types detected by *GALEX*: the absolute NUV magnitude has to be in the yellow region for the galaxy to be detected by *GALEX*. The detection limit corresponding to the MIS fields is shown by the dashed curve. The absolute NUV magnitude of the detected early types and their errors are shown by the blue points. Also shown is the expected evolution of the absolute NUV magnitude of a monolithic giant early-type galaxy ($M_V = -23$) that formed at $z = 3$ and has solar (*solid line*) and twice solar (*dashed line*) metallicity.

The average errors in the SDSS optical magnitudes are approximately 0.01 mag. The average uncertainty in the *GALEX* FUV and NUV magnitudes are ~0.25 and ~0.15 mag, respectively. The uncertainties in stellar population models are taken to be approximately 0.05 mag for optical passbands and 0.1 mag for the UV passbands (see Yi 2003). Since our observed sample contains galaxies at various redshifts, models are redshifted to $z = 0$ for each comparison, thus avoiding uncertainties due to *K*-corrections. The derived model fits are therefore in the *rest frame* of each observed early-type galaxy.

We use this procedure to derive best-fit values of (t_{YC}, f_{YC}) and χ^2 likelihoods in (t_{YC},f_{YC}) space for each galaxy. Our entire sample can be broadly divided into three categories. We illustrate this by showing the χ^2 contour maps of four example galaxies in Figure 8. The χ^2 minimum is marked with an x, and we indicate the 68% and 95% confidence contours. Galaxies 1 and 2 (*top row*) have clear signatures of RSF, since their 95% contours are contained completely within $t_{YC} < 1$ Gyr. Galaxy 3 shows a large age-mass degeneracy, which appears in most cases because the NUV flux from a small young starburst can be indistinguishable from that due to a larger but older starburst. Degenerate contours can also be the result of large errors in the observed photometry that allow many models to fit the data with values of (reduced) $\chi^2 < 2$. Therefore, even though galaxy 3 has a best-fit t_{YC} around 1 Gyr, we cannot rule out the possibility of younger or older populations being present, purely from its UV and optical photometry. Finally, galaxy 4 is likely to have old or intermediate age populations, since its 95% confidence contour lies exclusively at ages above 2 Gyr.

We note that, although they used a similar model for their analysis, the age-mass degeneracies in fits to our sample of galaxies are smaller than those studied by FS00. This is partly because optical uncertainties in SDSS measurements are 10 times smaller than those used by FS00. Together with the additional FUV constraint (FS00 only used rest-frame NUV), this allows a much smaller part of the (f_{YC}, t_{YC}) space to fit the colors of the observed early types.

In Figure 9 we summarize the *best-fit* values of (t_{YC}, f_{YC}) for our entire sample of galaxies. Red points indicate the best-fit values for early-type galaxies in our sample while orange points indicate best-fit positions of contaminants (galaxies that are rejected by the visual inspection or rejected by the AGN diagnostics). We find an increased scatter of contaminants toward lower values of t_{YC} (i.e., younger ages). We also show the 95% confidence contours of a galaxy with strong, moderate, and weak UV upturn (UVX) flux. We generate the strong UVX contour using the observed SED of NGC 4552. The moderate and weak UVX contours are computed by reducing the UV flux (<3500 Å) in the NGC 4552 SED by a factor of 2 and 6, respectively. In Figure 10 we show the distribution of best-fit t_{YC} values in our sample of galaxies—the inset shows the distribution of values restricted to the range $0 < t_{YC}^{\text{best-fit}} < 1$ Gyr. Figures 9 and 10 suggest that the UV + optical photometric properties of a significant number of early-type galaxies in our sample may not be compatible with a single rapid burst at high redshift followed by passive evolution. Such a conclusion is difficult to achieve with optical CMRs studied in the past (e.g., Bower et al. 1992, 1998; Ellis et al. 1997; Stanford et al. 1998; Gladders et al. 1998; van Dokkum et al. 2000), which are all consistent with purely passive monolithic scenarios.

We now classify our galaxies using their χ^2 contours, as follows: If the 95% confidence contour lies exclusively below a t_{YC} of 1 Gyr, then we label the galaxy as *young* (e.g., galaxies 1 and 2 in Fig. 8). If the 95% contour spans ages above and below 1 Gyr, the

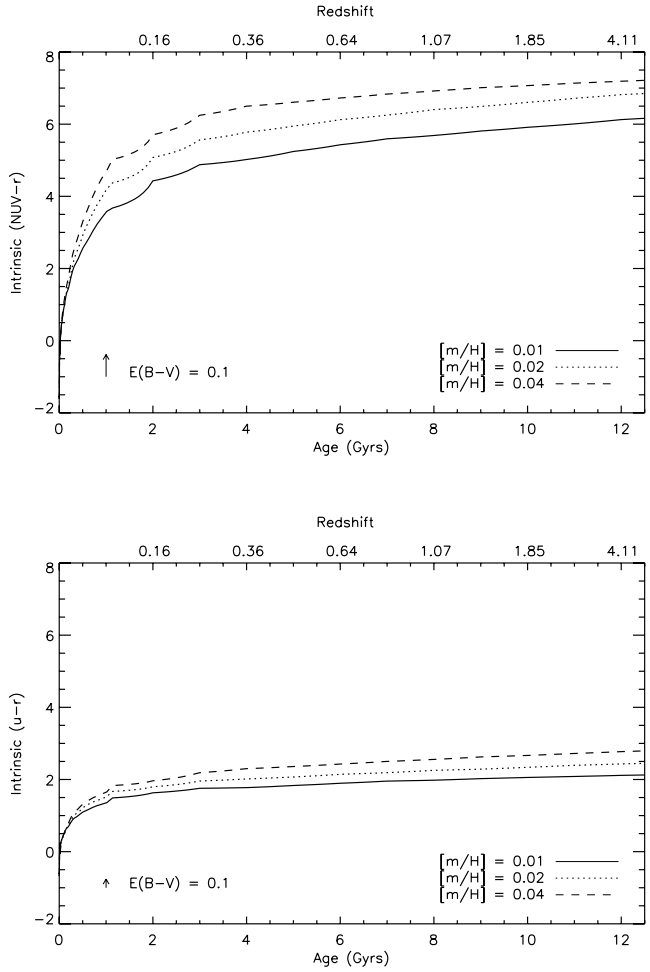

FIG. 7.—NUV − r (*top*) and $u - r$ (*bottom*) colors of a simple stellar population (SSP) as a function of age. The solid line shows SSPs with half solar metallicity, the dotted line represents solar metallicity, and the dashed line indicates twice solar metallicity. The evolution in the NUV − r color slows after 2 Gyr because the NUV flux from a recent starburst decays significantly in this timescale.

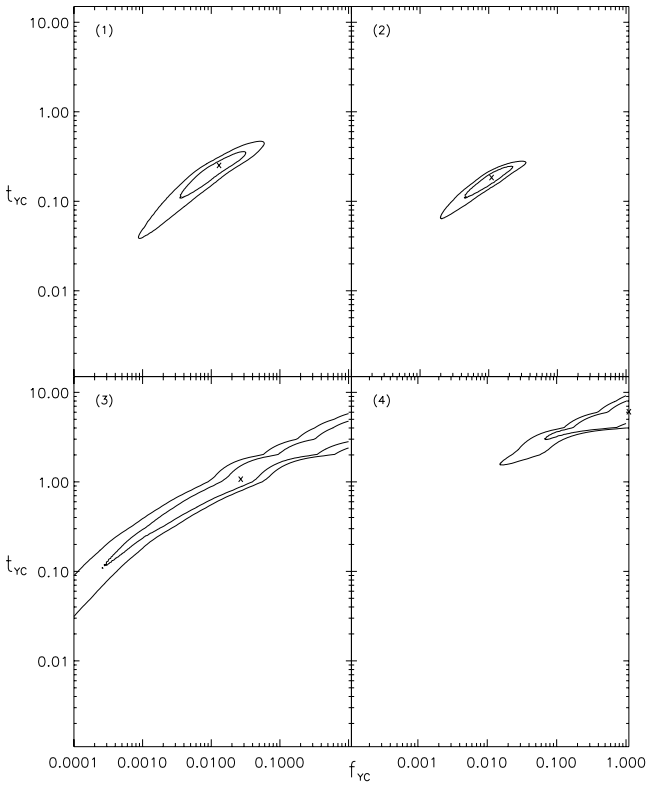

FIG. 8.—Four examples of χ^2 contour maps. The χ^2 minimum is marked with an x, and we indicate the 68% (1 σ) and 95% confidence contours. Galaxies 1 and 2 (*top row*) have clear signatures of RSF, since the 95% contours are contained completely within $t_{YC} < 1$ Gyr. Galaxy 3 shows a large age-mass degeneracy because the NUV flux from a small young starburst can be indistinguishable from a larger but older starburst. Finally, galaxy 4 is clearly likely to have old or intermediate age populations since its best-fit t_{YC} is greater than 3 Gyr and its 95% confidence contour does not extend far below 2 Gyr.

galaxy is classified as *degenerate* (e.g., galaxy 3 in Fig. 8). Finally, if the 95% contour lies exclusively above an age of 1 Gyr then the galaxy is classified as *old* (e.g., galaxy 4 in Fig. 8). As indicated in Figure 9, some galaxies have best-fit values that fall within the UVX contours defined by the observed SED of NGC 4552. These galaxies clearly have SEDs that resemble that of typical UV upturn galaxies but they may be initially labeled as *young*. However, since it is impossible to determine whether the shape of their SED is a result of RSF or UVX or a combination of both, we *relabel* these galaxies as degenerate.

In Figure 11, we plot the $u - r$ and NUV − r CMRs for the *GALEX* early types and color-code each galaxy using this classification scheme. We find that the optical CMR is unable to distinguish between different levels of RSF, since the various classifications cannot be distinguished in the optical CM space. However, the NUV CMR shows a clear *layered* structure. The galaxies classified as *young* (*blue symbols*) are bluest in the NUV − r colors and clearly separated from the *old* locus (*red symbols*) and *degenerate* class of galaxies (*green symbols*) forming an intermediate layer. Blue galaxies reside almost exclusively below NUV − $r \sim 5.5$ (for comparison, the NUV − r color of NGC 4552 is 5.4). Degenerate and old galaxies lie almost exclusively above NUV − $r \sim 5.5$.

We note that this method indicates the presence of RSF in a very general sense. Two instantaneous starbursts are clearly an oversimplification of the true SFH of early-type galaxies. The position of a galaxy in (f_{YC}, t_{YC}) space is a function of the *shape* of its SED and our efforts in this section have centered on approximating the shape of the true SED of each galaxy (using a library of f_{YC} and t_{YC}) through color fitting. Although the quantities f_{YC} and t_{YC} do not have a direct physical meaning, the two-starburst method probes whether there has been *any* star formation in these systems within the last Gyr. Since our classifications take account of the 95% confidence contours, i.e., the part of the parameter space that enclose 95% of the probability, we are able to derive conclusions about the presence of such RSF at the 95% confidence level. Having identified the signature of RSF in an object, we must then appeal to the various formation paradigms (see §§ 5 and 6 below) to motivate the star formation that generates the observed RSF.

4. THE BLUE FRACTION

Galaxies classified as young and shown in blue in Figure 11 are systems with a clear signature of RSF. In Figure 12 we show a stacked likelihood map of all blue galaxies, constructed by adding the likelihood maps of individual blue galaxies (see Fig. 8, *top row*) together. The black region indicates the part of parameter space where the average likelihood is higher than 95%. The dark and light gray regions correspond to regions where the probability is between 70% and 95% and 30% and 70%, respectively. Thus, the black region represents the values of f_{YC} and t_{YC} that

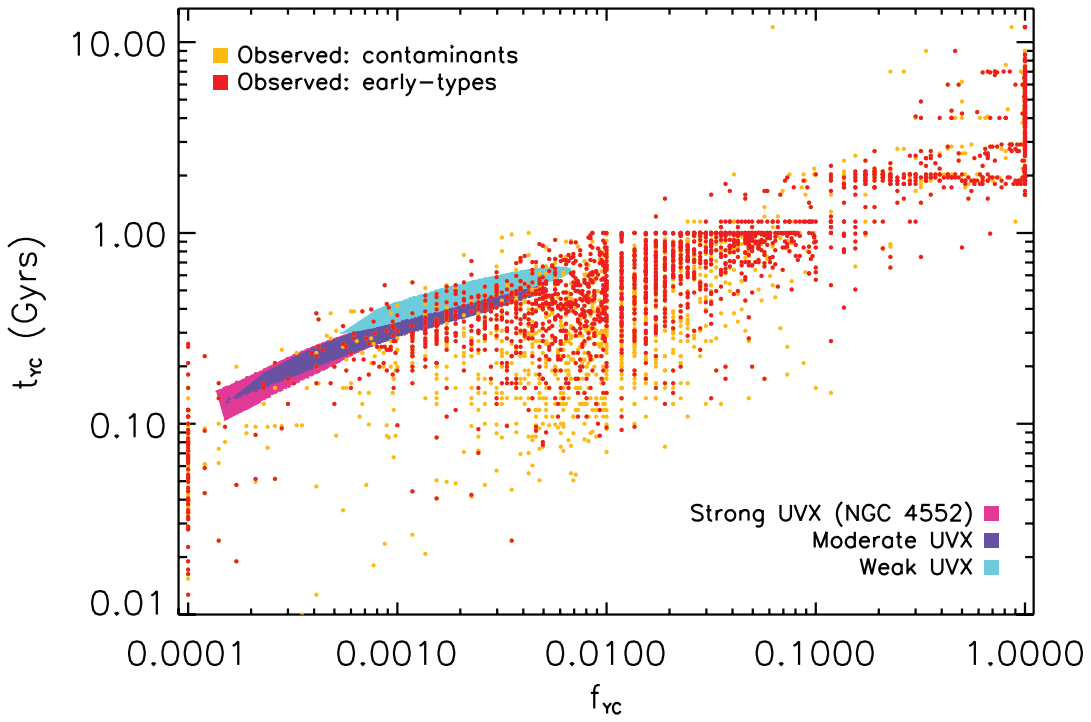

FIG. 9.—Best-fit values of $f_{\rm YC}$ and $t_{\rm YC}$, derived from fits to a simple model where the star formation history of each galaxy is described by two instantaneous bursts. The first burst occurs at $z = 3$, while the second burst is allowed to vary in age ($t_{\rm YC}$) and mass fraction ($f_{\rm YC}$). The model is described in detail in § 3.

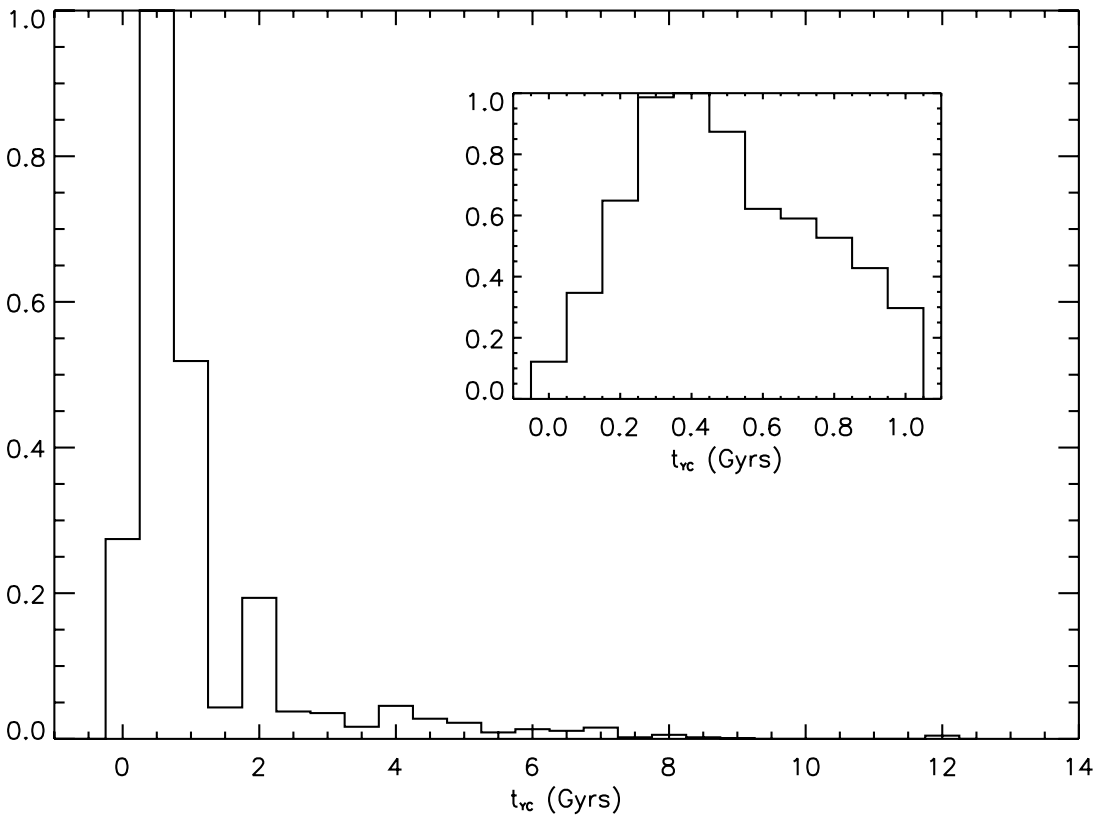

FIG. 10.—Distribution of best-fit $t_{\rm YC}$ values in our sample of galaxies-the inset shows the distribution of values restricted to the range $0 < t_{\rm YC}^{\rm best\text{-}fit} < 1$ Gyr.

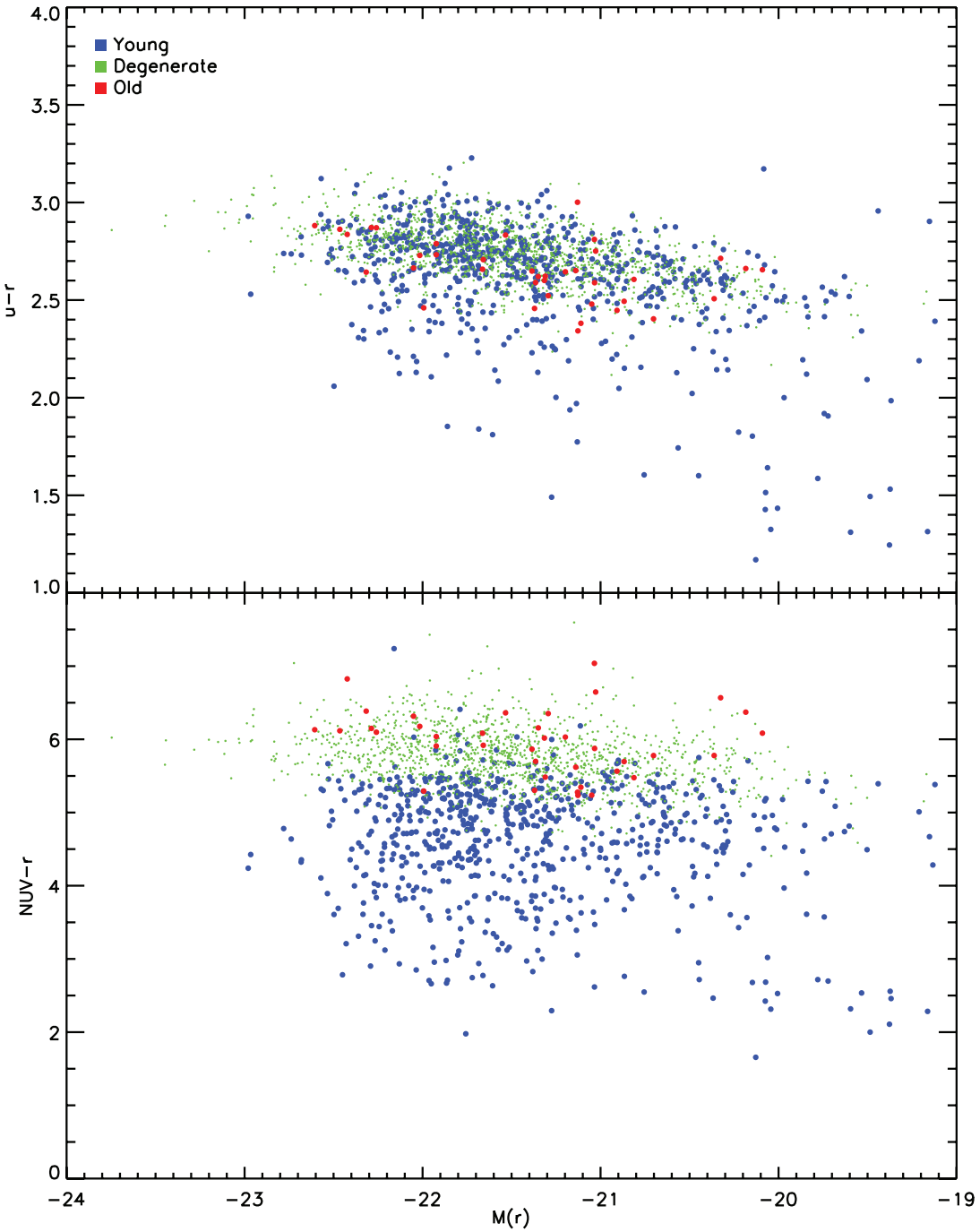

FIG. 11.—Optical $u - r$ CMR (*top panel*) and the NUV CMR (*bottom panel*) for the *GALEX* early types color-coded using the following classification scheme: if the 95% confidence contour does not extend to ages higher than 1 Gyr then the galaxy is classified as *young* (e.g., galaxies 1 and 2 in Fig. 8); if the 95% confidence contour spans ages below and above 1 Gyr, the galaxy is classified as *degenerate* (e.g., galaxy 3 in Fig. 8); if 95% confidence contour lies exclusively above an age of 1 Gyr, then the galaxy is classified as *old* (e.g., galaxy 4 in Fig. 8). *Young* galaxies are shown in blue, *intermediate* galaxies are shown in green and *old* galaxies are shown in red. Note that the photometry has not been *K*-corrected because this requires the assumption of a template—it is evident that an old passively evolving population is not good template for the local early-type population, at least for UV photometry.

are, on average, most likely for the blue population. The most likely value of $f_{\rm YC}$ is $\sim$1% and $t_{\rm YC}$ is $\sim$0.5 Gyr.

In Figure 13, we split the NUV CMR into narrow redshift bins and indicate the blue population in each bin. It is apparent from Figure 13 that, as a result of constructing an (apparent) magnitude limited sample, we are not sampling identical parts of the luminosity function at different redshifts. Comparing the blue fraction across our redshift range is therefore meaningful only for the part of the luminosity function that is sampled completely at all redshifts. Looking at the highest redshift bin, this appears to be for galaxies with $M(r) < -21.3$.

In Figure 14, we plot the evolution of the blue fraction with redshift. Recall that $\sim$10% of early-type galaxies in the SDSS sample remain undetected by *GALEX* (Fig. 6). The true value of the blue fraction should take these galaxies into account. We therefore assume that none of the nondetections are blue and adjust the blue fraction accordingly. This is a fairly strong assumption because the undetectability of these galaxies is a function of both their dust

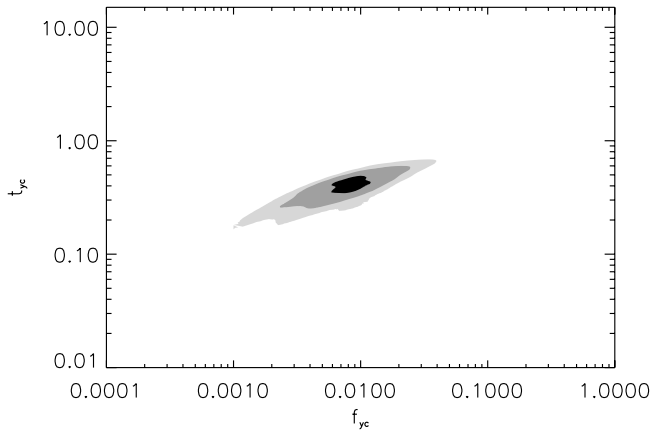

FIG. 12.—Stacked likelihood map of blue galaxies, constructed by adding the likelihood maps of each blue galaxy together. The black region indicates the region in which the average likelihood is higher than 95%. The dark and light gray regions correspond to regions in which the probability is between 70% and 95% and 30% and 70%, respectively. The black region represents the values of f_{YC} and t_{YC}, which are, on average, most likely for the blue population.

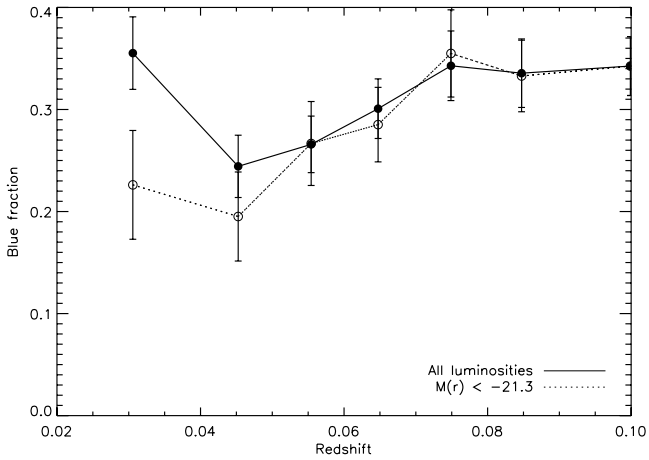

FIG. 14.—Evolution of the blue fraction with redshift. The solid curve takes into accounts all galaxies in each redshift bin (see Fig. 13), while the dotted curve considers only galaxies with $M(r) < -21.3$. Note that, due to arguments given in § 4, the blue fraction presented here is a *conservative estimate*.

content and metallicity. It is possible that some of these galaxies do have star formation but are heavily dust-reddened and/or metal-rich. Nevertheless, without their UV photometry this is a question we cannot answer.

The solid curve in Figure 14 takes into account all galaxies in each redshift bin, while the dotted curve considers only galaxies with $M(r) < -21.3$. Note also that at very low redshifts ($z < 0.05$), SDSS has a *bright* detection limit; spectroscopy is not possible for bright galaxies ($M(r) < -22.7$) that are extremely close ($z < 0.05$). Hence we do not properly sample the luminosity function in the first two redshift bins, although the blue *fraction* should remain unchanged due to this undersampling. The red curve in Figure 14 indicates that the fraction of blue systems for bright galaxies ($M(r) < -21.3$) varies between ~27% and 34% with an average value of ~30%. Within the errors there is negligible evolution in the blue fraction within the redshift range $0 < z < 0.11$. Nevertheless, both these points make our blue fraction a *conservative estimate*.

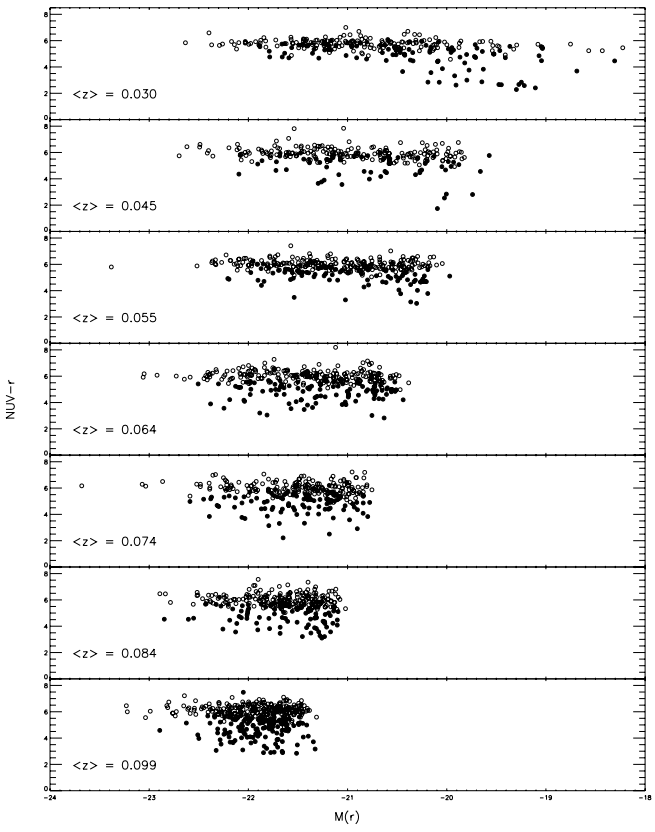

FIG. 13.—Evolution of the NUV CMR with redshift. Galaxies classified as *young* in the color-fitting analysis are shown by filled circles.

It is worth noting that the blue fraction computed in this study is a *lower limit* on the fraction of early-type galaxies that contain RSF. It is possible that some of the galaxies classified as degenerate also contain a certain level of RSF, but this is impossible to verify given their photometry and/or observational uncertainties. In addition, we have assumed that undetected ellipticals are not blue, although it is clearly possible that they *have* some star formation but are heavily dust-reddened or very metal-rich. This is, however, unquantifiable, and any correction to the blue fraction could be expected to be negligible within errors.

5. COMPARISON TO THE MERGER PARADIGM

Since we have established that RSF *does* exist in a significant fraction of the early-type population, it is natural to ask whether the properties of our local early-type sample can be reproduced in the currently popular hierarchical merger paradigm. We therefore explore the predicted NUV CMR in the semianalytical framework using the GALICS model, which combines large-scale *N*-body simulations with analytical recipes for the dynamical evolution of baryons within dark matter halos. We direct readers to H03 for specifics regarding the fiducial model. Kaviraj et al. (2005a) have used this model to accurately reproduce the observed optical CMR in cluster early-type galaxies in the redshift range $0 < z < 1.27$ (see their § 2). We use the blind UV predictions from this *optically calibrated model* to study the colors of the *GALEX* early-type sample. Note that galaxy morphologies in the model are defined by the ratio of *B*-band luminosities of the disk and bulge components, which correlates well with Hubble type (Simien & de Vaucouleurs 1986). A morphology index is defined as

$$I = \exp(-L_B/L_D), \quad (2)$$

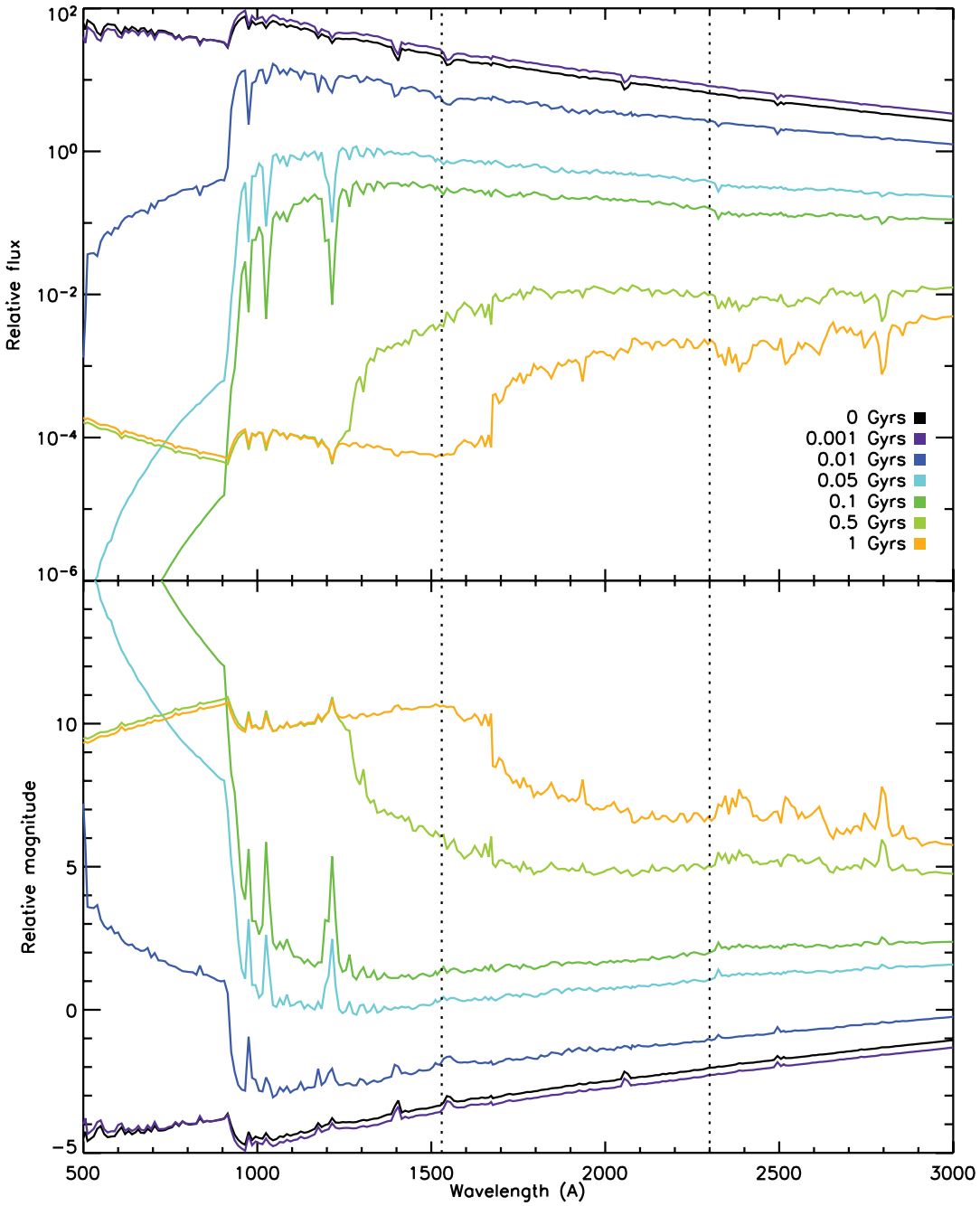

FIG. 15.—Evolution of the UV flux with age. *Top*: Relative UV fluxes of simple stellar populations. *Bottom*: Relative magnitudes of simple stellar populations shown in the top panel. The dotted lines indicate the peak throughput of the FUV and NUV filters. All models assume solar metallicities and are taken from the public BC2003 distribution.

so that pure disks have $I = 0$ and pure bulges have $I = 1$. Following Baugh et al. (1996), early-type galaxies have $I < 0.507$.[13]

We approach the problem from the point of view of reproducing the $(\mathrm{NUV} - r)$ *color distribution* using an ensemble of model galaxies in the redshift range spanned by the observed sample. In traditional (optical) CMR studies, the color distribution is often parameterized by the slope and scatter of the correlation. This is useful because the optical correlations are typically *tight*, i.e., have small scatter. But since the NUV CMR has more structure than can be expressed through the slope and scatter alone, matching only the slope and scatter within errors (which are large due to the significant dispersion in colors) is no longer sufficient.

5.1. *Treatment of Very Young Stars*

Since we are modeling the UV spectrum in this study, we must address some additional issues regarding the flux from (very) young stars in the model. The evolution of UV flux with the age of the UV-emitting young stars is highly nonlinear. Figure 15 shows the evolution of the UV spectrum with age, on both flux and magnitude scales for a solar metallicity stellar model from the public Bruzual & Charlot (2003) distribution. It is apparent that the UV flux of a 1 Myr population is ~4–5 *orders of magnitude* greater than that of a 1 Gyr population. Like other models of galaxy formation, star formation in GALICS is essentially proportional

[13] In this scheme ellipticals have $I < 0.219$, S0s have $0.219 < I < 0.507$ and spirals have $I > 0.507$.

to the cold gas available in the galaxy. Stars are therefore produced *continuously*. In addition, the GALICS model provides high age resolution (1 Myr) for very young stars. Therefore in a significant number of galaxies, a residual fraction of very young stars ($<$10 Myr old) is present.

There are two main issues regarding such young stars. Very young stars are typically embedded in birth clouds (BCs). During this embedded phase the attenuation due to dust in the ambient ISM is compounded by the dust present in the outer H I envelopes of the BCs. Thus, for embedded stars, the combined optical depth due to the BC and the interstellar medium (ISM) can be several times larger than due to the ISM alone (e.g., Charlot & Fall 2000). While most studies suggest that birth clouds are transient features with lifetimes of a few tens of Myr (e.g., Blitz & Shu 1980; Hartmann et al. 2001), a recent work (Scoville & Wilson 2004) suggests that the low efficiency of star formation in these clouds implies significantly longer lifetimes ($\sim$100 Myr). Recently formed stars may still migrate early from such long-lived BCs, since the BCs feel hydrodynamic forces, while the stars do not. However, the low gas density in early-type galaxies imply lower hydrodynamical forces, which could mean that migration timescales are longer (N. Scoville 2006, private communication).

In this study we apply a differential extinction scheme, in which the extinction applied to flux from embedded stars is a factor μ greater than the extinction felt by stars that are not embedded—calculated from the mean H column density (see H03, § 6.2). The key ingredients in this scheme are the factor μ and the age limit $\tau_{\rm max}$ of stars that are considered to be embedded. Following the studies mentioned above, we experiment with various values of $\tau_{\rm max}$ in the range 10–100 Myr and a range of values of μ between 3 and 10. We note that Charlot & Fall (2000) suggest $\langle\mu\rangle \sim 3$, albeit with a large scatter at lower and higher values; however, this is mainly for starbursting galaxies that have significantly different star formation histories than the early-type galaxies in our sample (see also Kong et al. 2004).

A second issue regards the modeling of star formation itself. Star formation is modeled as a continuous process proportional to the mass of cold gas in the system—as long as there is gas to fuel star formation, there are always some newborn, i.e., zero-age stars predicted in the model at *any* epoch. However, the question is whether, when galaxies are observed, *true zero-age stars* or indeed very young stars are actually seen. In reality, star formation is unlikely to be an idealized continuous process but probably occurs in random bursts of varying strengths and durations. Galaxies are therefore observed sometime *in between* two starbursts; i.e., there is a small *time delay* between a galaxy's most recent starburst and the point at which it is observed. For example, NGC 205, an "actively" star-forming dwarf elliptical (e.g., Burstein et al. 1988; Wilcots et al. 1990; Dorman et al. 1995; Bertola et al. 1995) in which the two most recent starbursts occurred $\sim$20 and $\sim$500 Myr ago (Wilcots et al. 1990), is noticeably bluer in UV-optical colors than other elliptical galaxies (Burstein et al. 1988). This suggests that it may not be correct to model *all* early-type galaxies with very young stars ($<$20 Myr old).

If we assume that starbursts in real galaxies are randomly, i.e., Poisson distributed, in time, then the distribution of time delays between starbursts is exponential.[14] The shape of the exponential is determined by the number of starbursts per Gyr (κ). In addition, the time lag distribution must be truncated at some value $l_{\rm max}$, since the time lag should generally be small and could have a minimum value $l_{\rm min}$ (e.g., $l_{\rm min} = 20$ Myr and $l_{\rm max} = 500$ Myr, from the NGC 205 arguments above). In this study we explore the (κ, $l_{\rm min}$, $l_{\rm max}$) parameter space for values of $l_{\rm min}$ in the range 0–0.05 Gyr and $l_{\rm max}$ in the range 0.2–0.5 Gyr. We assume that $\kappa = 10$, i.e., that a starburst has, on average, a timescale of $\sim$0.1 Gyr, so that galaxies tend to have $\sim$10 bursts per Gyr.

[14] This is a general property of Poisson distributions.

5.2. *Reproducing the NUV CMR in the Merger Paradigm*

A one-to-one comparison between the model and observed photometry requires that the two samples are consistent in terms of the magnitude and redshift ranges covered by each. We therefore take the following points into account while performing our comparisons:

1. From Figure 14 we see that, due to the magnitude limit of our observed sample, luminosity function coverage is complete only for galaxies brighter than $M(r) = -21.3$. We therefore restrict our comparison *only* to real and model galaxies with $M(r) < -21.3$.
2. As mentioned above, the SDSS spectroscopic sample has a *bright limit*—bright galaxies that are very close do not have spectroscopy and therefore do not appear in our observed sample. A large sample of galaxies drawn from the SDSS DR3 indicates that this bright limit lies around $M(r) = -22.7$ for $z < 0.05$. We therefore remove such galaxies from the model sample.
3. The *GALEX* detection limit (m(NUV) < 23) implies that some galaxies predicted in the model will not be "*GALEX*-detectable'." The comparison must therefore include only model galaxies that are *GALEX*-detectable.
4. A fourth point that does not particularly affect our comparison but is worth noting is that the model itself has a completeness limit (see § 8.2 and Table 3 of H03), because small halos are not fully resolved in the simulation due to the mass resolution of GALICS.[15] The completeness limit for GALICS in r band is around -20.4. While the effects of such a lack of resolution may propagate over the formal completeness limit of -20.4, this does not affect our comparison if we restrict ourselves to $M(r) < -21.3$, since this is well within the completeness threshold.
5. Finally, all model SEDs are redshifted to present day before the comparison, to avoid uncertainties due to K-corrections. This is important, because without robust low-redshift templates for the UV spectra of early-type galaxies, we cannot reliably estimate UV K-corrections-we have already established that a purely passively evolving template does not match at least 30% of the early-type galaxies at low redshifts. Later in this section we present UV K-corrections based on the photometry of our best-fit models.

We generally find that reproducing the observed photometry without invoking time lags is difficult. The assumption of moderate BC survival spans ($\sim$10–50 Myr) leaves the model photometry with roughly correct scatter but with a zero-point that is consistently too blue, regardless of how heavily attenuated the flux from young stars is. To illustrate this point we show, in Figure 16, the case in which $\mu = 10$ and $\tau_{\rm max} = 50$ Myr; i.e., the BC + ISM extinction is 10 times that of the ISM alone and BCs survive for 50 Myr. Note that, for clarity, in this and other similar figures that follow, we draw a random sample of model galaxies that has the same size as the observed sample. While the top panel of Figure 16 indicates that the scatter is reasonably reproduced, the color distributions in the bottom panels show that the zero-point

[15] In GALICS the merging history is driven by the N-body *backbone* on which galaxies are "painted." The mass resolution is therefore determined by the mass of the dark matter particles ($\sim 10^{10}\,M_{\odot}$). Other models (e.g., Benson et al. 2000; Khochfar & Burkert 2003) use the Press-Schechter formalism (Press & Schechter 1974), with theoretically infinite resolution, so that the merging history of even the smallest objects is fully resolved.

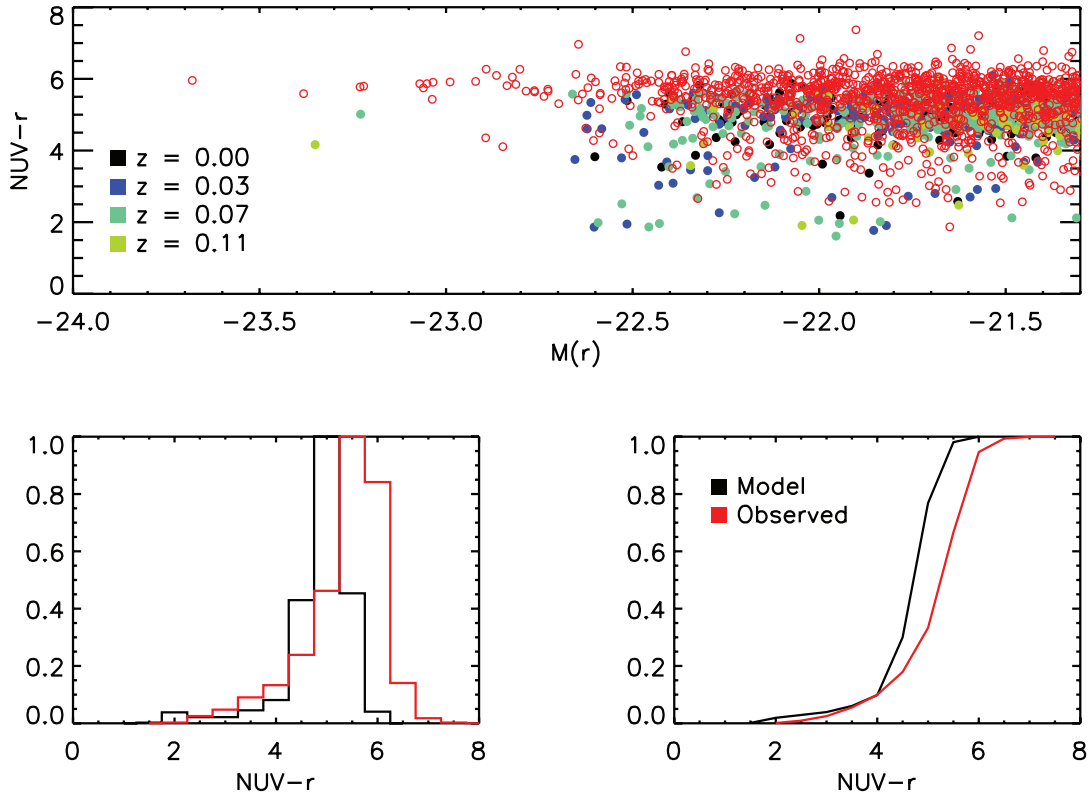

FIG. 16.—Comparison of observed and model photometry in the case in which $\mu = 10$ and $\tau_{max} = 50$ Myr; i.e., the BC + ISM extinction is 10 times that of ISM alone and BCs survive for 50 Myr. The open red circles represent the observed photometry. All other colors represent model galaxies at various redshifts (see legend in plot). The bottom panels condense the information shown in the top panel. The plot on the bottom left shows the NUV − r color distribution and the plot on the bottom right shows the cumulative NUV − r color distribution.

of model photometry is clearly too blue by ∼0.5 mag in such a scenario.

The situation can be significantly improved by invoking longer BC lifetimes close to 100 Myr (i.e., $\tau_{max} = 100$ Myr). Figure 17 shows the BC lifetime distribution we adopt in this study. It is highly skewed toward an upper limit of 100 Myr. Figure 18 shows the comparison between the observed results and the models based on this assumption along with a BC extinction which is 5 times that due to the ISM alone. We find that this comparison gives a reasonable fit to the photometry, although as mentioned before, it is unclear whether recently formed stars within BCs linger within them for the lifetime of the cloud itself.

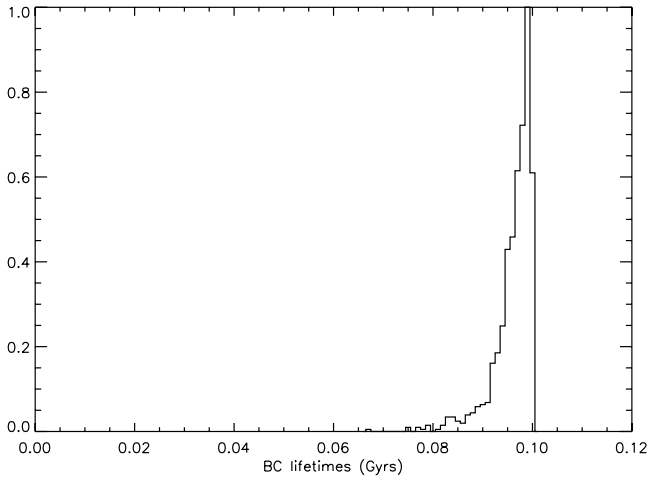

FIG. 17.—Exponential distribution of BC lifetimes employed to produce the comparison shown in Fig. 18.

Invoking small time lags into the model photometry, *while keeping BC lifetimes short*, produces similar results. The observed photometry can be reproduced best if we assume a minimum time lag of 20 Myr (e.g., NGC 205 arguments given above), a maximum time lag of ∼200–300 Myr and an exponential time lag distribution constructed on the assumption that galaxies have, on average, 10 starbursts per Gyr. We also assume that stars less than 30 Myr old reside in BCs and experience 3 times the extinction due to the ISM alone (e.g., Charlot & Fall 2000). Using the terminology of § 5.1 this translates to $\mu = 3$, $\tau_{max} = 30$ Myr, $\kappa = 10$, $l_{min} = 20$ Myr, and $l_{max} = 200$ Myr. Note that the BC + ISM extinction only affects stars that are between 20 and 30 Myr old since, by construction, there are no stars younger than 20 Myr in this model (since $l_{min} = 20$ Myr). This comparison is shown in Figure 19. Henceforth, we refer to this scenario as the best-fit model. As might be expected, the goodness of fit is more sensitive to the minimum time lag l_{min}-scenarios where $l_{min} < 20$ Myr make both the zero-point too blue and the scatter too large to fit the observations. The fit is less sensitive to the maximum time lag but we use $l_{max} = 200$ Myr, the lowest value of l_{max} that gives a good fit.

As the bottom panels of Figure 19 indicate, the best-fit scenario reproduces the color distribution of the observed sample well. The evolution of the (complete) NUV CMR in this scenario is shown in Figure 20. Note that the number of galaxies in each redshift bin is around ∼6000. The red dots indicate galaxies that are below the detection limit of *GALEX*; i.e., they are not *GALEX*-detectable.

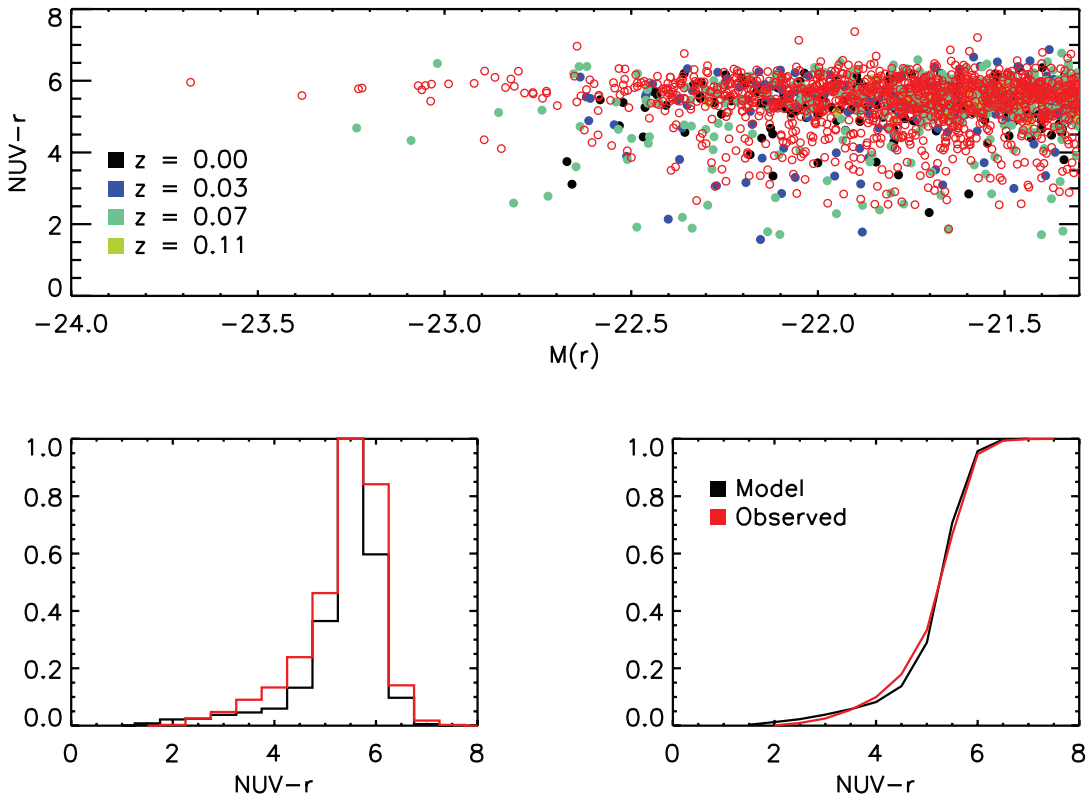

FIG. 18.—Comparison of observed and model photometry in the case in which an exponential distribution of BC lifetimes is employed (see Fig. 17). The extinction assumed due to the BCs is 5 times that due to the ISM alone; i.e., $\mu = 5$. The open red circles represent the observed photometry. All other colors represent model galaxies at various redshifts (see legend in plot). The bottom panels condense the information shown in the top panel. The plot on the bottom left shows the NUV $-$ r color distribution and the plot on the bottom right shows the cumulative NUV $-$ r color distribution.

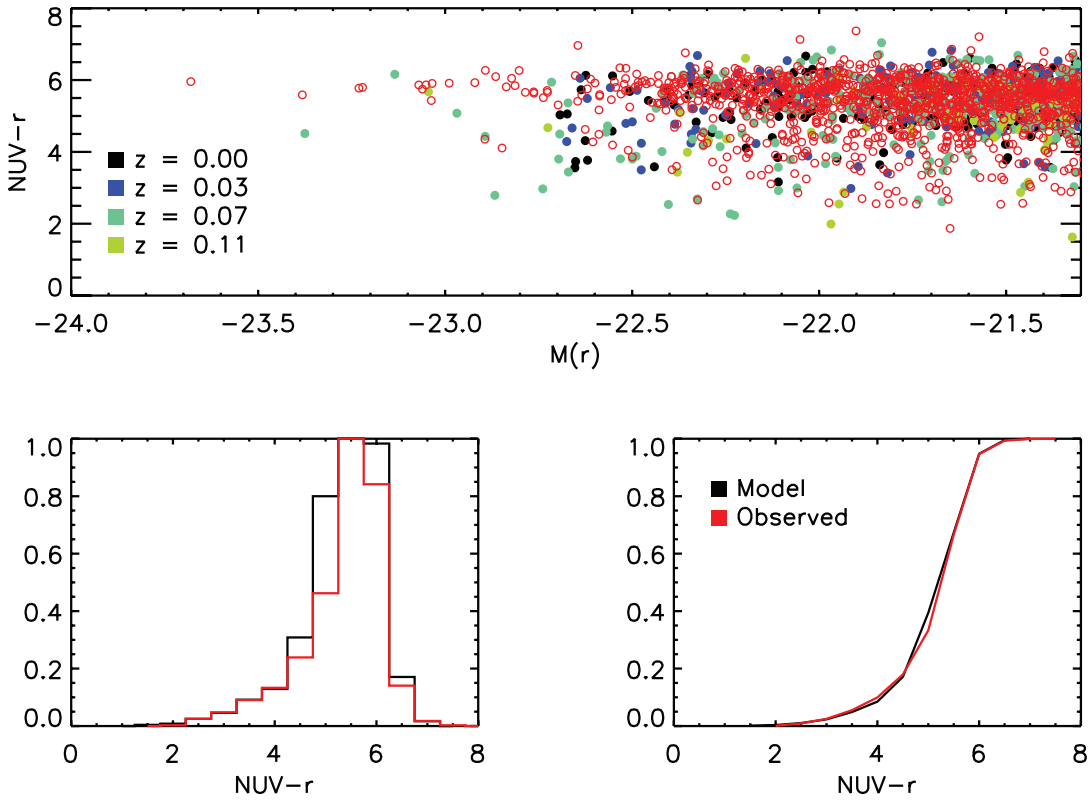

FIG. 19.—Comparison of observed and model photometry in the best-fit model where $\mu = 3$, $\tau_{max} = 30$ Myr (see Charlot & Fall 2000) $l_{min} = 20$ Myr and $l_{max} = 200$ Myr. The open red circles represent the observed photometry. All other colors represent model galaxies at various redshifts (see legend in plot). The bottom panels condense the information shown in the top panel. The plot on the bottom left shows the NUV $-$ r color distribution and the plot on the bottom right shows the cumulative NUV $-$ r color distribution.

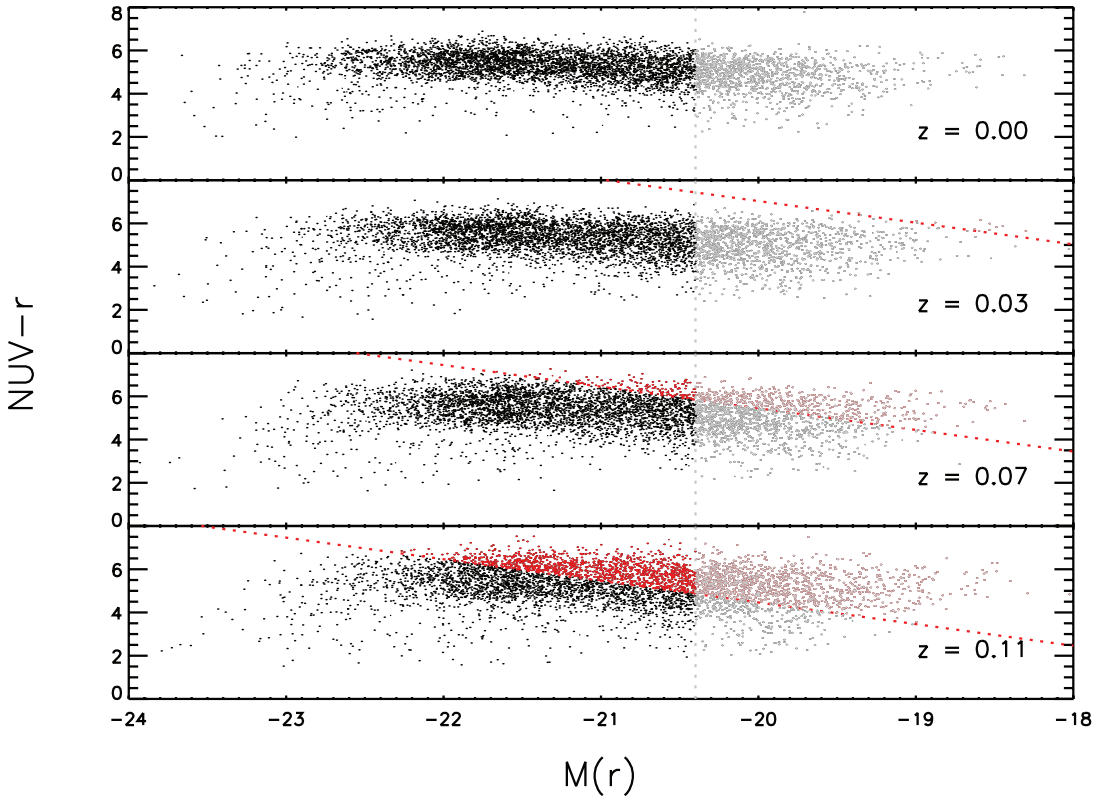

FIG. 20.—Evolution of the NUV CMR in the best-fit model. The red dots indicate galaxies that are below the detection threshold of *GALEX*. The gray dots lie in the region below the completeness limit of the GALICS model. The detection limit encroaches severely on the model sample at the upper end of our redshift range ($z = 0.11$).

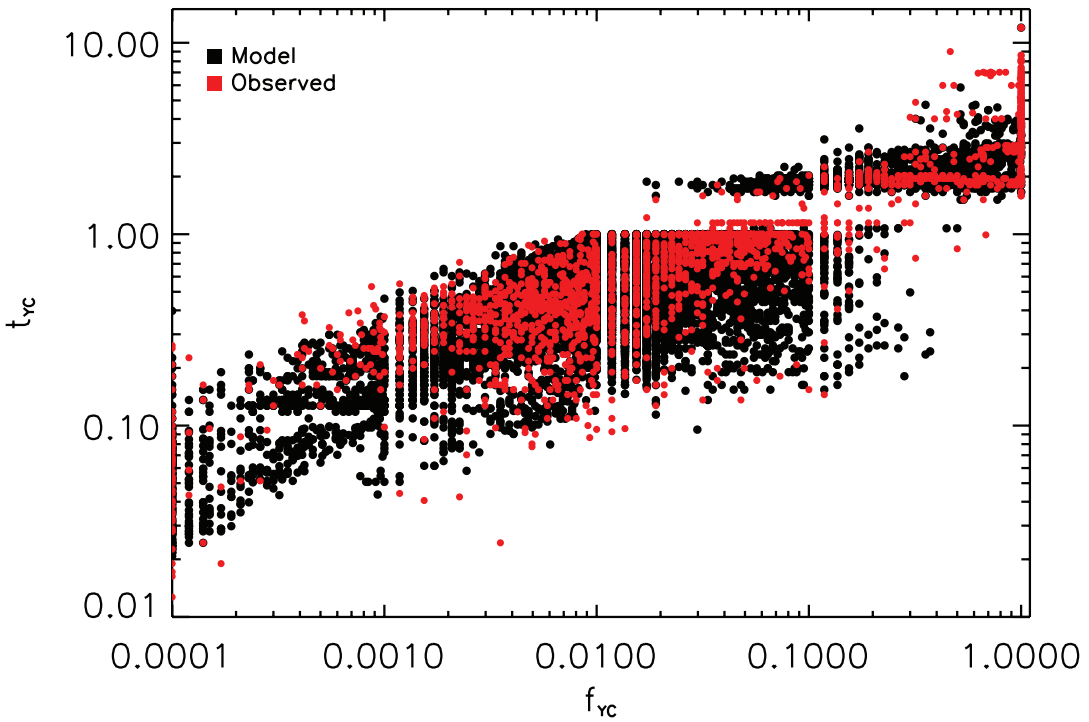

FIG. 21.—Two-component method applied to model early types in the GALICS hierarchical merger model that is used in this study. Black points represent model galaxies, and the red points represent the observations. Note that this comparison is not restricted to galaxies with $M(r) < -21.3$. All observed galaxies and all model galaxies above the completeness limit of $M(r) = -20.4$ are plotted. There are no significant systematic differences between the positions of model and observed galaxies in this parameter space, implying that the observed photometry across the UV and optical spectral ranges is reproduced reasonably well by the models.

TABLE 2
AVERAGE PROPERTIES OF RECENT STAR FORMATION IN MODEL EARLY TYPES

z	$\langle f \rangle$	$\langle \tau_m \rangle$	$\langle \tau_v \rangle$	$\langle \tau_r \rangle$
0.03	0.014	0.61	0.55	0.55
0.07	0.021	0.62	0.55	0.57
0.11	0.025	0.50	0.37	0.38

NOTES.—$\langle f \rangle$ is the average RSF mass fraction, i.e., the stellar mass fraction within the last Gyr. $\langle \tau_x \rangle$ is the average age of this RSF fraction, in Gyr, weighted by the quantity indicated in the subscript x. Subscript m indicates mass, v indicates V-band luminosity and r indicates r-band luminosity. These values are derived from the best-fit model (Fig. 19), which produces excellent quantitative agreement with the UV-optical photometry of the nearby early-type galaxies studied in this paper.

The gray dots lie in the region below the completeness limit of the GALICS model. The detection limit encroaches severely on the model sample at the upper end of our redshift range ($z = 0.11$).

While it is apparent that the best-fit model reproduces the UV photometry of the observed sample, we now apply the two-component analysis used in § 3 to the predicted photometry from the best-fit model. The position of an object in ($f_{\rm YC}$, $t_{\rm YC}$) space is a direct function of the *shape* of its SED, which in turn drives its photometric properties both in the UV and the optical spectral ranges. A comparison, in this parameter space, between the positions of the model galaxies and the observed population indicates the overall robustness of the fit, not only in terms of the NUV color but in terms of the shape of the complete SED. The derivation of ($f_{\rm YC}$, $t_{\rm YC}$) for model galaxies uses the same process as that used for the observed sample. We show this comparison in Figure 21. Note that we show all available galaxies in the observed sample and similarly all model galaxies above the GALICS completeness limit—we do not restrict the analysis to galaxies with $M(r) < -21.3$. We find that there are no systematic differences between the positions of model and observed galaxies in this parameter space, which implies that the observed photometry across the UV and optical spectral ranges is reproduced reasonably well by the best-fit model. Table 2 summarizes the properties of the recent star formation in the galaxies in the best-fit model. On average, low-redshift early-type galaxies are predicted to have ~1.5%–2.5% of their stellar mass formed within the last Gyr. The mass-weighted age of this star formation is between 0.4 and 0.6 Gyr, and its luminosity-weighted average age is around 0.5 Gyr.

We end this section by computing K-corrections from our best-fit models. As suggested by our previous analysis, purely old, passively evolving populations are clearly *not* adequately good templates for the UV spectra of early-type galaxies, even though the UV emission in these galaxies is weak. In Figure 22, we show K-corrections for UV colors from our best-fit model in the redshift range spanned by our observed sample (*black dots with error bars*). We also compare these K-corrections to those obtained from a passively evolving 9 Gyr old SSP (*dashed lines*) and the elliptical template from the Kinney spectral atlas of galaxies (*dotted lines*; Kinney et al. 1996). The use of a 9 Gyr SSP is motivated by the fact that Bernardi et al. (2003d) find that their early-type sample can be best fit by a 9 Gyr passively evolving SSP, formed at high redshift.

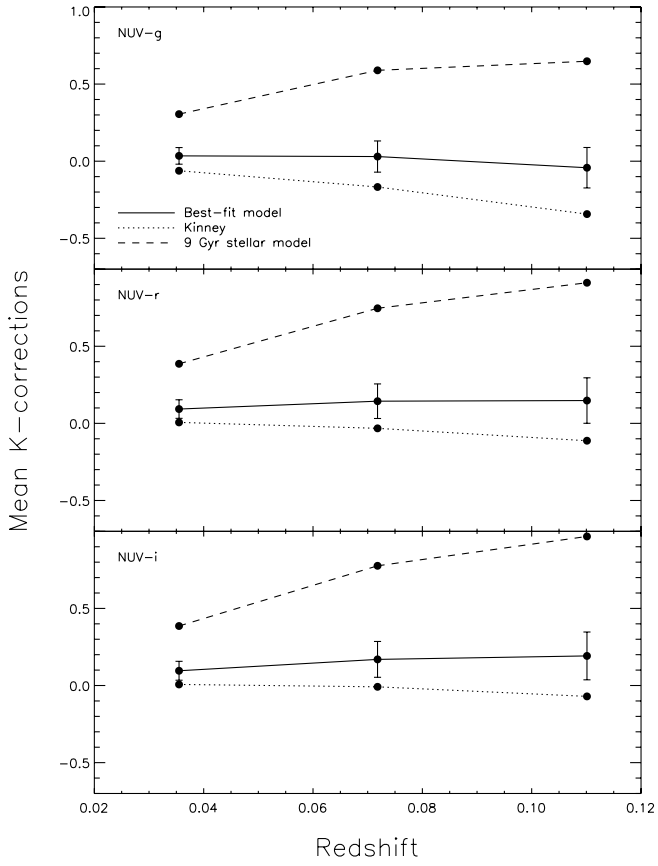

FIG. 22.—K-corrections for UV colors from our best-fit model in the redshift range spanned by our observed sample (*solid line*). Also shown are K-corrections obtained from a passively evolving 9 Gyr old stellar model (*dashed line*) and the elliptical template from the Kinney spectral atlas of galaxies (*dotted line*).

5.3. *The Role of Mergers and Progenitor Bias*

In this section we briefly present certain salient features of the semianalytical modeling used to match the observed UV-optical photometry, which illustrates the origin of the UV flux in the predicted early-type populations. Although it represents a small diversion from the main theme of the paper, this sections outlines the mechanics of early-type galaxy formation within the framework of the model, especially the evolution at recent look-back times that are most relevant to the UV-flux generation within these systems.

Star formation in the merger paradigm proceeds through one of two channels—*quiescent* star formation governed by the mass of available cold gas and the dynamical timescale of the galaxy (H03, § 4.1) or *merger-driven* star formation as a result of dynamical interactions between galaxies (H03, § 5). As Figure 23 indicates, it is possible for galaxies to have experienced very recent mergers, within the last Gyr of look-back time. The top panel in Figure 23 shows the redshifts of the *most recent* mergers experienced by early-type galaxies at $z = 0$. These are essentially the *dynamical ages* of these galaxies, i.e., the epoch at which the galaxy in its present (morphological) form was created. The bottom panel shows the average trend in dynamical ages as a function of luminosity (size). In a hierarchical picture of galaxy formation larger early types are assembled later, i.e., have smaller dynamical ages, although the ages of their stellar populations are, on average, older (Kaviraj et al. 2005a).

We investigate the impact such recent mergers may have on the color of the early-type remnants, and the extent to which they may affect the blue colors exhibited by some early-type galaxies. In Figure 24, we compare the UV color distribution of galaxies that have experienced recent mergers (within the last Gyr), with the global color distribution of all early-type galaxies. We find that recent mergers do not have a preponderance of blue galaxies, suggesting that *mergers at low redshift are predominantly dry and not the cause for the blue scatter* in the UV colors of early-type

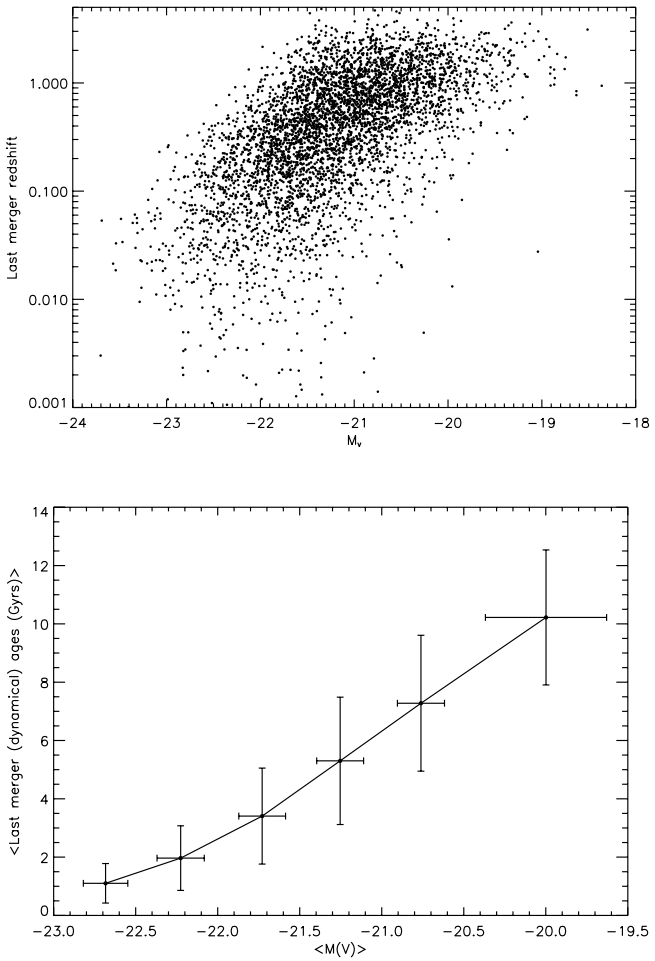

FIG. 23.—*Top*: Redshifts of most recent mergers experienced by early-type galaxies at $z = 0$. These are essentially the *dynamical ages* of these galaxies, i.e., the epoch at which the galaxy in its present (morphological) form was created. *Bottom*: Average dynamical ages of galaxies as a function of their luminosity (size). As expected, in a hierarchical picture of galaxy formation, larger galaxies are assembled later, i.e., have smaller dynamical ages, although the ages of their stellar populations are, on average, older (Kaviraj et al. 2005a).

galaxies—star formation from the quiescent mode is at least as important as that due to mergers.

We finish this section by briefly mentioning the issue of progenitor bias, which affects all studies of early-type galaxies at $z > 0$, in the framework of the merger paradigm. Fundamental to merger-driven morphological transformations is the implication that, at higher redshifts, a progressively larger fraction of mass that eventually resides in present-day early types is potentially locked up in late-type systems (van Dokkum & Franx 2001). Like all other early-type studies, this investigation has attempted to trace the evolution of the *local* early-type population by looking *only at their early-type progenitors in the redshift range* $0 < z < 0.11$. Any non-early-type progenitors have been excluded, for the simple reason that it is not possible to easily identify them. Although we expect progenitor bias to be smallest at low redshifts (indeed this is the big advantage of studying *nearby* early-type galaxies), it is instructive to quantify this effect and gauge its possible impact on the blue fraction derived in § 4.

The top panel in Figure 25 indicates the extent of progenitor bias by plotting the fraction of the $z = 0$ early-type galaxies that have already undergone their last merger and assumed their final early-type morphology as a function of redshift. At $z \sim 0.1$, roughly 10% of present-day early-type galaxies are still "in pieces." If, for example, these "pieces" were blue late-type systems, then we could have underestimated the blue fraction in § 4. However, we have already shown (Fig. 24) that recent mergers in this redshift range have a similar UV color distribution to the rest of the population, i.e., that recent mergers are not preferentially bluer. Indeed, mergers at low redshift have a high probability of involving at least one early-type progenitor (Fig. 25, *bottom*). Note that our results are consistent with Khochfar & Burkert (2003), who were the first to present a detailed analysis of the progenitor morphologies of early-type galaxies. Thus, since progenitor bias is small within our redshift range and mergers tend to be dry, neglecting non-early-type progenitors will not affect the blue fraction derived in this study.

6. REVISITING THE MONOLITHIC HYPOTHESIS

The monolithic hypothesis remains the simplest and perhaps most elegant explanation for a remarkably wide range of properties of large early-type galaxies (e.g., Peebles 2002). Indeed, a careful treatment using *N*-body/SPH simulations (Chiosi & Carraro 2002; Tantalo & Chiosi 2002) suggests that monolithic formation can reproduce a wide spectrum of chemophotometric properties of large early types. Until now these properties have been restricted to the optical spectrum. The UV photometry presented in this paper provides, for the first time, a new constraint on the formation of such large early-type systems. While it is apparent that a merger-based treatment is able to reproduce the UV + optical photometry of local early types fairly accurately, the RSF mass fractions (∼1%–3%) involved are small. The presence of young stars in these galaxies indicates that there is fuel, i.e., cold gas, available for star formation at low redshift. It is, therefore, natural to ask whether the required level of fuel *could* be supplied in a traditional monolithic scheme.

Monolithic models propose a high star formation efficiency at high redshift, which drives a violent episode of star formation resulting in the bulk of the galaxy forming within a short timescale at high redshift (e.g., $z < 2$). However, stars created in the primordial burst would *recycle* a fraction of their mass back into the ISM through stellar winds and supernova ejecta. A fraction or all of this internally recycled gas *could* fuel further star formation, without invoking any external gas accretion or interactions. The aim of this section is to investigate whether, given reasonable assumptions for the evolution and chemical enrichment of such a monolithic system, we can reproduce the RSF and the observed UV photometry of large early-type systems *that form part of the blue fraction*.[16] The reason for restricting ourselves to large blue galaxies is because, as mentioned before, red galaxies *can* be reconciled with a monolithic scenario, especially if we assume that part of the scatter in the red sequence is determined by varying levels of intrinsic dust in these galaxies. This monolithic analysis is useful because, if low-level star formation seen in the observed blue population can be produced simply by returned material from stars formed in the primordial burst, then there would, in principle, be no need to invoke a merger based scenario to produce early-type galaxy colors.

6.1. *Simulating Monolithic Collapse*

The model used here (see Ferreras & Silk 2000a) follows the standard chemical enrichment equations (e.g., Tinsley 1980).

[16] While we could simply explore the *amount* of recycled material expected in a typical monolithic simulation, it is necessary to simulate the accompanying chemical enrichment because the NUV − *r* color is a function of both the total amount and the metallicity of the recycled gas.

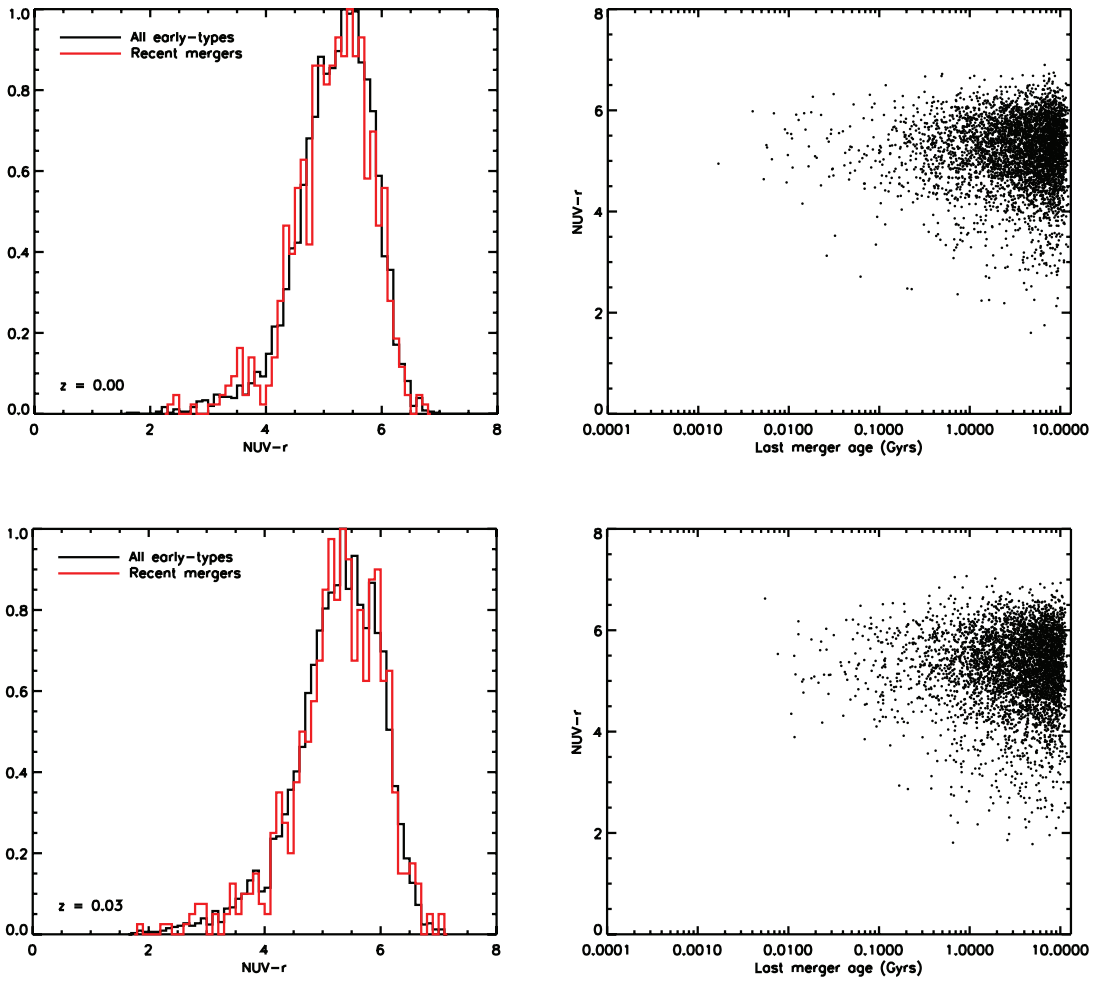

FIG. 24.—*Left*: Comparison between the UV colors of *model* early-type galaxies (from the best-fit model) that have had recent mergers (red) within the last Gyr of look-back time with the color distribution of all galaxies. *Right*: UV colors of model early-type galaxies as a function of their dynamical (last-merger) ages. The dynamical age is explained in the text and in the caption to Fig. 23. We find that recent mergers (e.g., within the last 1 Gyr) do not have a preponderance of blue galaxies, suggesting that mergers at low redshift are predominantly *dry* and not the cause for the blue scatter in the UV colors of early-type galaxies.

Stellar yields are taken from Thielemann et al. (1996) for stellar masses $M_* > 10\ M_\odot$ and from van den Hoek & Groenewegen (1997) for lower mass stars. We use a standard Salpeter IMF; note that we assume instantaneous recycling but *not* instantaneous mass loss, so that the lifetimes of stars of various masses is taken into account.

We simulate a scenario in which (Gaussian) gas infall, with a short timescale (~1 Gyr), occurs at "high" redshift. Most studies that support the monolithic hypothesis agree on a formation epoch somewhere before $z = 2$; it is difficult to pinpoint it any further using the available data. Our conclusions are not sensitive to the exact redshift of formation, so we use a fiducial value of $z = 3$. The formation redshift is taken as the epoch at which the gas infall *peaks*. The star formation rate is governed by the generally accepted Schmidt law (Schmidt 1959):

$$\Psi = Cg^{\alpha}, \tag{3}$$

where Ψ is the star formation rate, C is the star formation efficiency, g is the gas mass, and $\alpha = 1.5$.

We explore the behavior of the system using two free parameters. The first and most significant free parameter is the star formation efficiency C in equation (3). Low values of C result in more extended star formation, while high values of C result in faster consumption of gas and a shorter episode of star formation. Note that C is not numerically restricted to a value between 0 and 1. As expected, increasing C to arbitrarily high values does not result in the star formation increasing without limit, simply because the system cannot consume gas faster than it is being put in. We explore the behavior of the system in this limiting high- C regime, where star formation essentially tracks the gas infall very closely, i.e., as soon as gas becomes available, it is almost instantly converted to stars. As a result, the overwhelming bulk of the galaxy is already constructed by the time gas infall ends at high redshift, mimicking the fundamental feature of a monolithic collapse. However, star formation does not stop when gas infall ceases. Gaseous ejecta returned from dying stars is gradually released back into the ISM over a Hubble time, providing potential fuel for further star formation. It is the quantity of this recycled gas that we investigate here—in particular, we explore whether there is *enough* gas in this recycled material to fuel late stage star formation and reproduce the RSF mass fractions seen in large blue early types in our observed sample.

The second free parameter is a simple prescription for galactic winds, which is parameterized by assuming that a certain fraction (B) of gaseous ejecta is permanently lost from the system.

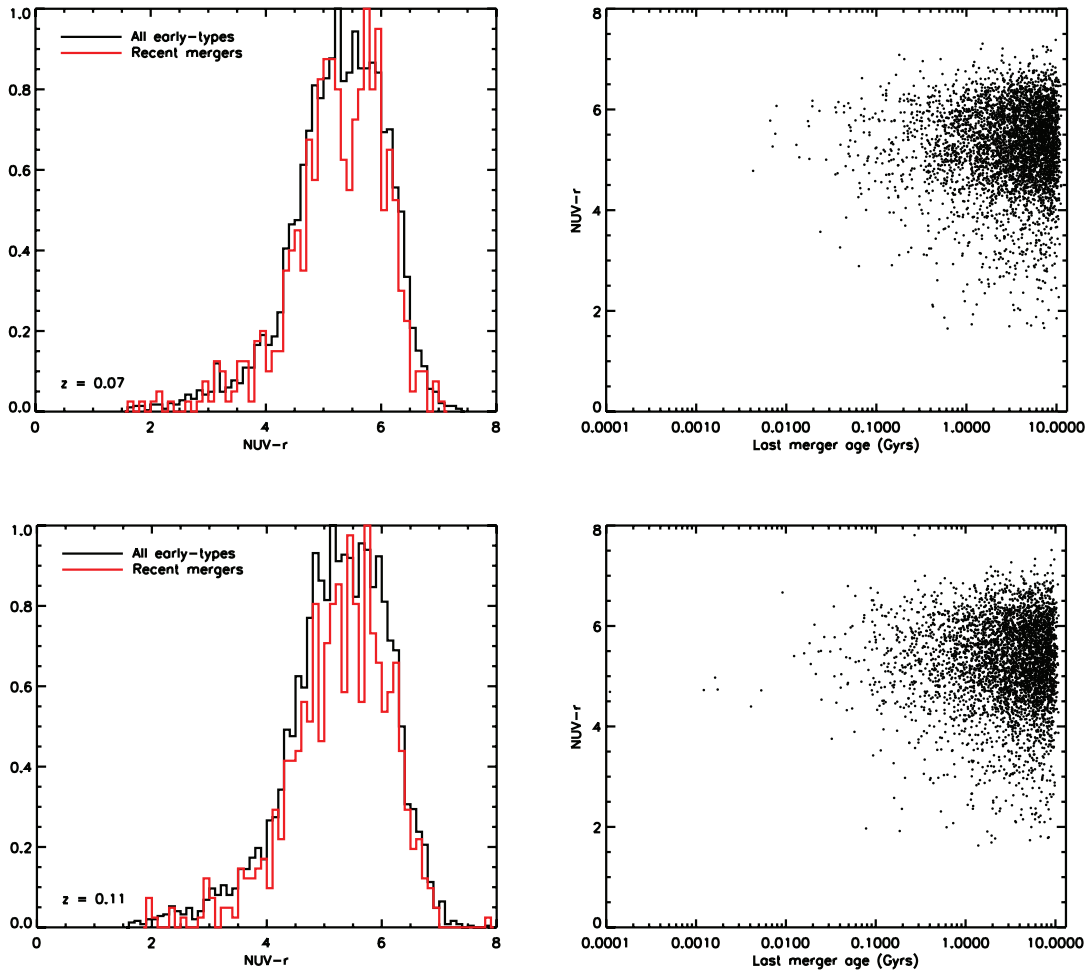

FIG. 24—*Continued*

B varies between 0 and 1. We are primarily interested in scenarios in which B is small, since we are exploring large early-type galaxies, which should have potential wells deep enough to retain most of the ejected gas. $B = 0$ corresponds to essentially closed-box evolution after the initial gas infall stage.

6.2. *RSF in Monolithic Early-Type Galaxies*

We begin by looking at the simplest scenario, where $B = 0$, i.e., all ejecta are retained by the system—this is also, of course, the scenario that *maximizes* the late stage returned gas fraction. The $B = 0$ scenario is summarized in Figure 26. The left-hand column shows the star formation rate (*top row*), gas infall (*middle row*), and the evolution of stars and gas (*bottom row*) for various values of C (see legend in the top row), with B fixed at 0. We note that the limiting high-C regime, which mimics monolithic collapse, is achieved for values of C above $\sim$100. Above this value, increasing C does not affect the SFR (*top row*), because the SFR is effectively limited by the rate of gas infall, since stars cannot be produced faster than gas is being deposited in the system. As mentioned before, increasing C allows the SFR to track the gas infall function more closely, as can be seen in Figure 26. The yellow SFR curve, which represents a system with high C, peaks almost coevally with the gas infall, whereas the black SFR curve, which represents the lower C regime, produces more extended star formation and has its peak significantly displaced from the peak of the gas infall. Our focus in this section is exclusively on the high-C regime ($C > 100$), in which star formation after the initial gas infall stage is fueled *only* by recycled gas.

The right-hand column in Figure 26 shows average quantities produced by such a scenario. The rows from top to bottom show the average age, average metallicity, average alpha enhancement, fraction of stars formed within the last Gyr (the RSF fraction), $u - r$ color, and NUV $- r$ color, respectively, as a function of C (with B fixed at 0). We also indicate, in the relevant rows, the average values (and their formal errors) of [m/H] and [Mg/Fe] computed by Trager et al. (2000a) for local early-type galaxies.[17] Figure 26 indicates that, in the $B = 0$ scenario, monolithic values of C ($C > 100$) predict present-day RSF fractions of <0.005. In comparison, we find that large ($>L_*$), blue (NUV $- r < 5.5$) galaxies in the merger models have present-day RSF fractions of $\sim$0.03. The monolithic RSF fraction, driven purely by the recycled material from stars, is generally a factor 5–6 lower than what is required, in a merger framework, to reproduce the colors of large, blue early-type galaxies in the observed sample.

It is instructive to explore the full range of values for B, although our exclusive interest in large galaxies implies that values of B should be low. As we show below, very high values of B

[17] Note that Trager et al. (2000a) find milder values of $\langle$[m/H]$\rangle$ and $\langle$[Mg/Fe]$\rangle$ than in previous studies (e.g., Weiss et al. 1995; Trager et al. 1997; Greggio 1997).

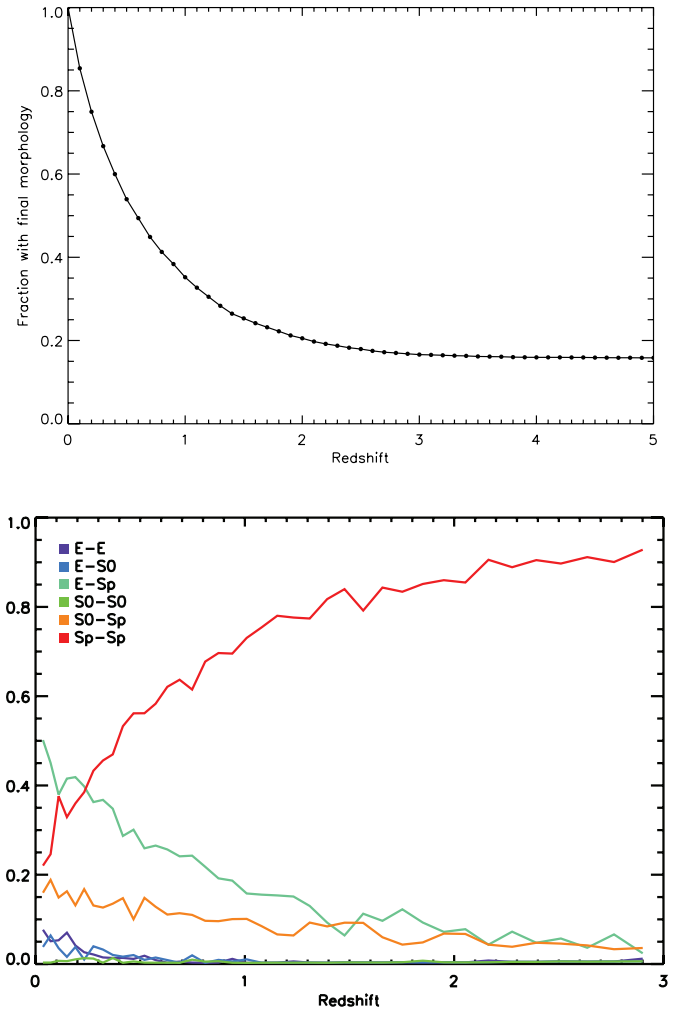

FIG. 25.—*Top*: Fraction of local ($z = 0$) early-type galaxies that have already attained their final (early-type) morphology, i.e., had their last merger, as a function of redshift. *Bottom*: Progenitor types in binary mergers. At low redshift mergers have a higher probability of having at least one early-type progenitor. See Khochfar & Burkert (2003) for a detailed analysis of the progenitor morphologies of early-type galaxies.

result in excessive metal loss, producing galaxies that are too metal-poor to fit the observed metallicities of local early types. To illustrate the trend in B we show, in Figure 27, the case in which $B = 0.3$; i.e., 30% of stellar ejecta are permanently lost from the galaxy. We find, in this case, that galaxies are generally more metal-poor than the mean relations derived by Trager et al. (2000a)—increasing B simply exacerbates this situation.

We summarize our investigation of monolithic models in Figure 28, which plots the NUV $-$ r color (*top left*), RSF fraction (*bottom left*), mean metallicity (*top right*), and mean [Mg/Fe] (*bottom right*) as a function of B and C. We find that, in the high-C regime ($C > 100$), which we take to be the traditional definition of monolithic collapse (see arguments above), models that fit the metallicity and alpha enhancement expected in local early-type galaxies generally do *not* produce the blue colors of large blue early types. Models with $B < 0.3$ reproduce the full spectrum of average metallicities and alpha-enhancements observed in large early-type galaxies. However, the NUV $-$ r color predicted by these models is typically above $\sim$6, because RSF fractions contributed by stars within the last Gyr (which dominate the UV flux) are too low ($<$0.005), compared with blue galaxies predicted in merger models ($\sim$0.03). To illustrate this, we compare, in Figure 29, a monolithic SFH ($B = 0$, $C = 100$) to the *average* SFH of large ($>L_*$), blue (NUV $-$ $r < 5.5$) early-type galaxies predicted in the merger model. The top panel shows the noncumulative SFH, while the bottom panel compares the cumulative SFH. Due to the inadequate RSF fractions, blue colors can *only* be produced in a traditional monolithic scheme by invoking high values of B, which leads to high metal loss and a metal-poor galaxy. However, such metal-poor models do not fit the observed metallicities of large early-type galaxies in the nearby universe.

It is, of course, conceivable that the expelled gas, parameterized by B, does not escape the galaxy potential well completely but is re-accreted by the galaxy over the dynamical timescale of the galaxy. However, recalling that stellar mass that dominates the rest-frame UV flux is created within the last Gyr of look-back time, we find that for reasonable dynamical timescales, expelled gas falling back into the galaxy will have a negligible effect. We illustrate this using a simple analytical argument. Assuming that the entire expelled fraction (B) falls back into

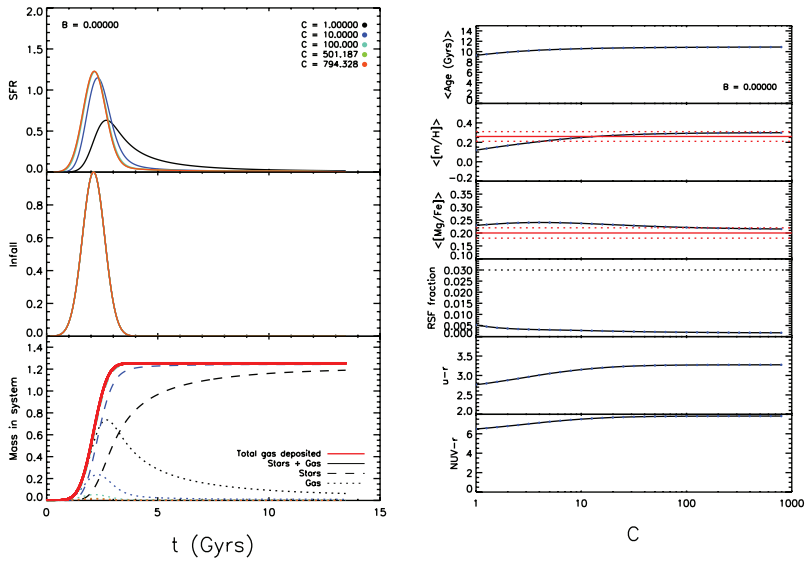

FIG. 26.—*Left-hand column*: Star formation rate (*top row*), gas infall (*middle row*), and the evolution of star and gas (*bottom row*) for B fixed at 0 and various values of C (see legend in the top row). *Right-hand column*: Average quantities-rows from top to bottom show average age, metallicity, alpha-enhancement, fraction of stars formed within the last Gyr (the RSF fraction), $u - r$ color and NUV $-$ r color, respectively, as a function of C (with B fixed at 0). Also indicated, in the relevant rows, are the average values of [m/H] and [Mg/Fe] computed by Trager et al. (2000a) for local early-type galaxies.

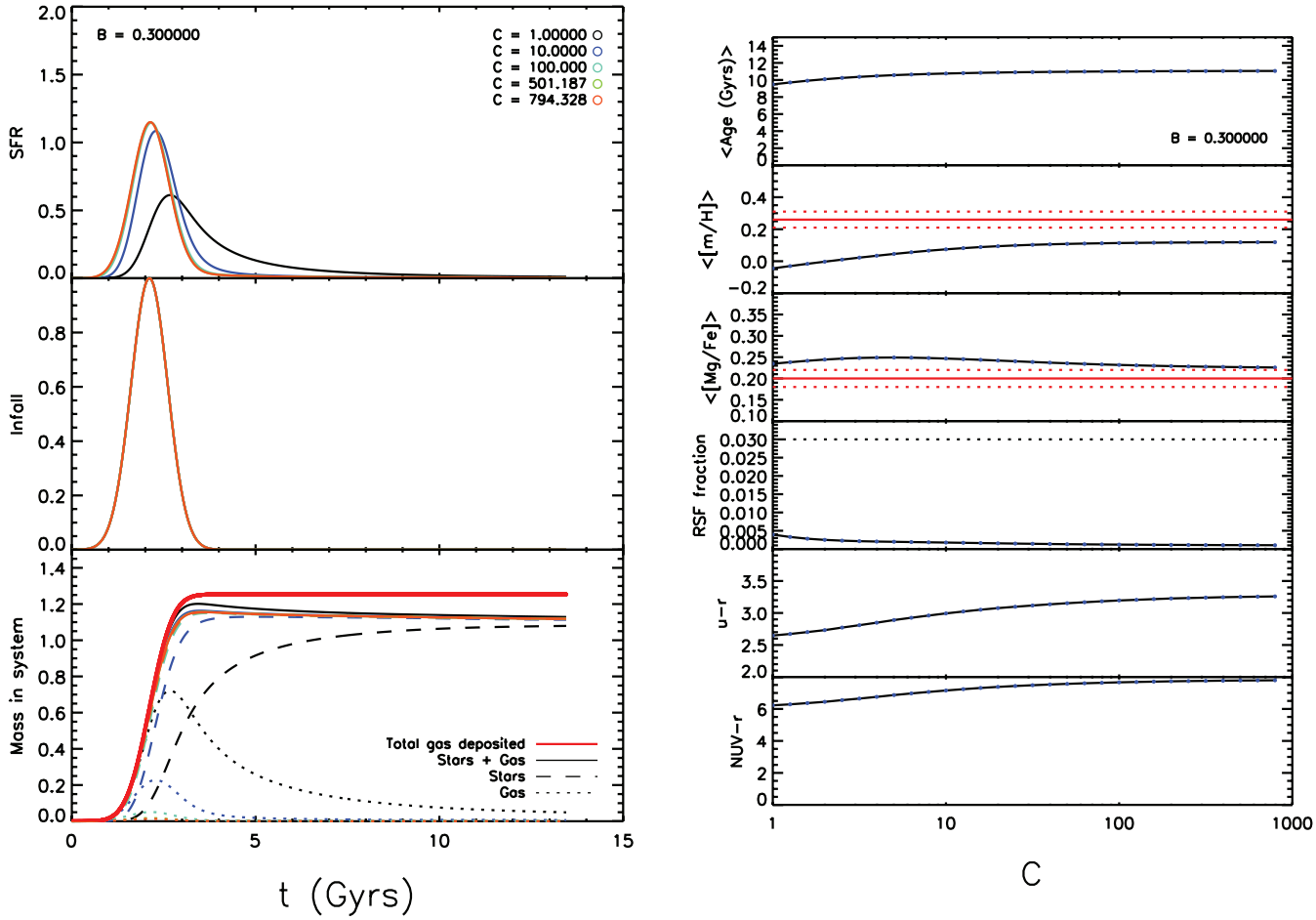

FIG. 27.—Same as Fig. 26 except for $B = 0.3$. *Left column*: Star formation rate (*top row*), gas infall (*middle row*) and the evolution of star and gas (*bottom row*) for B fixed at 0 and various values of C (see legend in the top row). *Right column*: Average quantities-rows from top to bottom show average age, metallicity, alpha-enhancement, fraction of stars formed within the last Gyr (the RSF fraction), $u - r$ color and NUV $- r$ color, respectively, as a function of C (with B fixed at 0.3). Also indicated, in the relevant rows, are the average values of [m/H] and [Mg/Fe] computed by Trager et al. (2000a) for local early-type galaxies.

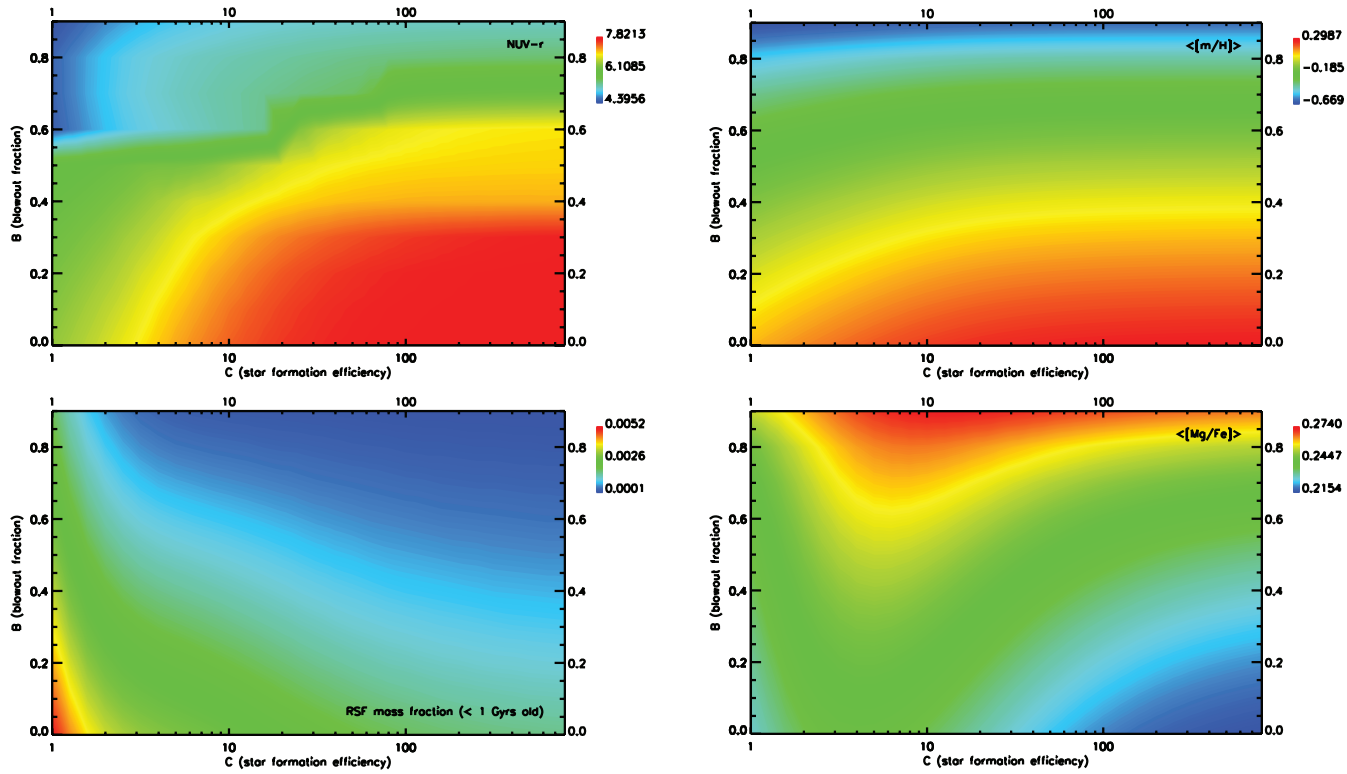

FIG. 28.—Summary of average quantities as a function of B and C: NUV $- r$ color (*top left*), RSF fraction (*bottom left*), mean metallicity (*top right*), and mean alpha-enhancement (*bottom right*).

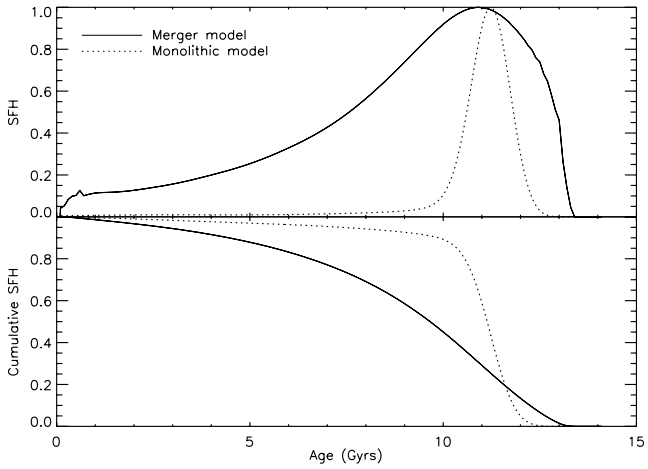

FIG. 29.—Comparison between a monolithic SFH and the average SFH of large ($>L_*$), blue (NUV $- r < 5.5$) early-type galaxies predicted by the merger model (which fit the colors of corresponding observed early-type galaxies). The top panel shows the noncumulative SFH, while the bottom panel compares the cumulative SFH.

the galaxy and that this reservoir of initially expelled gas empties exponentially, we have

$$g(t) = B \exp(-t/\tau), \quad (4)$$

where $g(t)$ is the expelled gas contained in the reservoir and τ is the dynamical timescale of the galaxy. Therefore, between times $t = t_1$ and t_2 the amount of gas falling into the galaxy is given by

$$g(\triangle t) = B[\exp(-t_1/\tau) - \exp(-t_2/\tau)]. \quad (5)$$

To make a significant impact on the UV color of the galaxy, this infalling material must contribute $\sim$3% of the stellar mass of the galaxy. Assuming that the infall of expelled gas starts promptly after the main mass of the galaxy is in place, i.e., $\sim$5 Gyr after the beginning of star formation (see Fig. 26), the gas that produces the UV emitting stars falls in between $t = 7$ and 8; assuming the universe is $\sim$13 Gyr old. Hence, UV emitting stars less than 1 Gyr old will form a stellar mass fraction approximately equal to

$$B[\exp(-7/\tau) - \exp(-8/\tau)], \quad (6)$$

which is required to be $\simeq$0.03, to produce the blue observed colors. However, it is difficult to achieve such mass fractions—reasonable dynamical timescales close to what is expected for large early-type galaxies ($\sim$1 Gyr) provide stellar fractions that are 2 orders of magnitude lower than the required $\sim$3%. The stellar fraction is maximum ($\sim$1.5%) for $\tau \sim 7$ Gyr, which is unrealistic for large early-type galaxies. Robust *observational* constraints on the amounts of recycled gas will aid the type of analysis presented in this section. Although recent studies (e.g., Young 2005), which compare the distribution of specific angular momenta of gas and stars, do indicate that at least some of the gas in early-type galaxies is created from stellar mass loss, it is still unclear what fraction of the detected gas may have an *external* origin.

In particular, the fraction of gas that is internally produced (and therefore shares the kinematics of their source stars) must be eventually correlated with the integrated UV fluxes from these systems, to determine whether the total observed UV flux can be accounted for by internally sourced gas alone—such a study is currently in progress using *GALEX* and SAURON data and results may become available in the near future (M. Bureau 2006, private communication).

However, based on the analysis presented in this section, we conclude that monolithic evolution, where RSF is driven *solely* by recycled gas from stellar mass loss, is not a viable channel for the production of large blue early-type galaxies.

7. CONCLUSIONS

We have studied $\sim$2100 early-type galaxies in the SDSS DR3 that have been detected by the *GALEX* medium depth (MIS) survey, in the redshift range $0 < z < 0.11$. The early-type sample has been selected through careful morphological inspection, with potentially UV-contaminating AGNs removed through the use of both optical spectral data (from the SDSS) and radio data (from the VLA FIRST survey). At a 95% confidence level, *at least* $\sim$30% of early-type galaxies in this sample have optical and UV photometry consistent with *some* recent star formation within the last Gyr.

Our analysis indicates that, while optical CMRs cannot distinguish between early-type galaxies that have had star formation within the last Gyr and those that have not, the NUV CMR is an excellent diagnostic of RSF—any galaxy with NUV $- r < 5.5$ has a high likelihood of containing recent star formation (RSF), even after taking into account the possibility of a contribution to the NUV spectrum from UV upturn flux.

Comparison of the observations to predictions of a semianalytical ΛCDM hierarchical merger model yields good quantitative agreement (across the UV and optical spectrum), if we assume that (1) very young stars ($<$30 Myr old) are contained in birth clouds that increase dust extinction by a factor of $\sim$3 compared to the ISM alone and (2) that star formation is driven by random (pseudo-instantaneous) starbursts that are Poisson distributed in time, so that there is a small time lag between the last starburst and the observation of the galaxy—the time lags are distributed exponentially in time, with maximum and minimum values of 200 and 20 Myr, respectively.

Combining our parametric analysis of the UV + optical photometry of the observed early types, with the properties of the predicted population in the semianalytical model, we conclude that early-type galaxies in the redshift range $0 < z < 0.11$ are likely to have $\sim$1%–3% of their stellar mass in stars less than 1 Gyr old. The (V-band luminosity weighted age) of this recent star formation is $\sim$300–500 Myr.

Finally, we find that monolithically evolving galaxies, where RSF can be produced solely from recycled gas due to stellar mass loss, do not exhibit the blue colors (NUV $- r < 5.5$) seen in some large early-type galaxies in our observed sample. While the degeneracy between the monolithic and merger paradigms cannot be broken for red early types even with UV photometry, a monolithic scenario is a very unlikely channel for the evolution of large blue early-type systems. Such blue galaxies require *additional* fuel for star formation, which must necessarily have an external origin.

We are grateful to the anonymous referee for various clarifications. We warmly thank Chris Wolf for providing high-resolution COMBO-17 images, which formed an integral part of our morphological classification process. We also thank Mariangela Bernardi for her generous help in the initial stages of this project,

for providing the DR2 versions of her SDSS early-type catalog prior to publication, and many interesting discussions. We are grateful to Jeremy Blaizot for his extensive help with the GALICS model and to Andrés Jordán, Joseph Silk, Roger Davies, and Andrew Benson for many useful comments regarding this work. S. K. acknowledges PPARC graduate DPhil scholarship PPA/S/S/2002/03532. This work was supported by grant R01-2006-000-10716-0 from the Basic Research Program of the Korea Science & Engineering Foundation and Yonsei University Research Fund (2005) to S. K. Y.

REFERENCES

Baldwin, J. A., Phillips, M. M., & Terlevich, R. 1981, PASP, 93, 5 (BPT81)
Baugh, C. M., Cole, S., & Frenk, C. S. 1996, MNRAS, 283, 1361
Becker, R. H., White, R. L., & Helfand, D. J. 1995, ApJ, 450, 559
Bell, E. F., et al. 2004, ApJ, 608, 752
Benson, A. J., Cole, S., Frenk, C. S., Baugh, C. M., & Lacey, C. G. 2000, MNRAS, 311, 793
Bernardi, M., & the SDSS collaboration. 2003a, AJ, 125, 1817
———. 2003b, AJ, 125, 1849
———. 2003c, AJ, 125, 1866
———. 2003d, AJ, 125, 1882 (B03)
Bertola, F., Bressan, A., Burstein, D., Buson, L. M., Chiosi, C., & di Serego Alighieri, S. 1995, ApJ, 438, 680
Bica, E., & Alloin, D. 1987, A&AS, 70, 281
Blitz, L., & Shu, F. H. 1980, ApJ, 238, 148
Boselli, A., et al. 2005, ApJ, 629, L29
Bower, R. G., Kodama, T., & Terlevich, A. 1998, MNRAS, 299, 1193
Bower, R. G., Lucey, J. R., & Ellis, R. 1992, MNRAS, 254, 589
Bruzual, G., & Charlot, S. 2003, MNRAS, 344, 1000
Burstein, D., Bertola, F., Buson, L. M., Faber, S. M., & Lauer, T. R. 1988, ApJ, 328, 440
Butcher, H., & Oemler, A. 1984, ApJ, 285, 426
Caldwell, N., Rose, J. A., & Concannon, K. D. 2003, AJ, 125, 2891
Calzetti, D., Armus, L., Bohlin, R. C., Kinney, A. L., Koornneef, J., & Storchi-Bergmann, T. 2000, ApJ, 533, 682
Charlot, S., & Fall, S. M. 2000, ApJ, 539, 718
Chiosi, C., & Carraro, G. 2002, MNRAS, 335, 335
Cole, S., Lacey, C. G., Baugh, C. M., & Frenk, C. S. 2000, MNRAS, 319, 168
Couch, W. J., Barger, A. J., Smail, I., Ellis, R. S., & Sharples, R. M. 1998, ApJ, 497, 188
Deharveng, J.-M., Boselli, A., & Donas, J. 2002, A&A, 393, 843
Deharveng, J.-M., Jedrzejewski, R., Crane, P., Disney, M. J., & Rocca-Volmerange, B. 1997, A&A, 326, 528
Dorman, B., O'Connell, R. W., & Rood, R. T. 1995, ApJ, 442, 105
Dressler, A. 1980, ApJ, 236, 351
Dressler, A., et al. 1997, ApJ, 490, 577
Ellis, R. S., Smail, I., Dressler, A., Couche, W. J., Oemler, A. J., Butcher, H., & Sharples, R. M. 1997, ApJ, 483, 582
Falcón-Barroso, J., & the SAURON collaboration. 2006, MNRAS, 369, 529
Ferreras, I., Scannapieco, E., & Silk, J. 2002, ApJ, 579, 247
Ferreras, I., & Silk, J. 2000a, ApJ, 532, 193
———. 2000b, ApJ, 541, L37 (FS00)
Fukugita, M., Nakamura, O., Turner, E. L., Helmboldt, J., & Nichol, R. C. 2004, ApJ, 601, L127
Gladders, M. D., Lopez-Cruz, O., Yee, H. K. C., & Kodama, T. 1998, ApJ, 501, 571
Greggio, L. 1997, MNRAS, 285, 151
Hartmann, L., Ballesteros-Paredes, J., & Bergin, E. A. 2001, ApJ, 562, 852
Hatton, S., Devriendt, J. E. G., Ninin, S., & Bouchet, F. R. 2003, MNRAS, 343, 75 (H03)
Hodge, P. W. 1973, ApJ, 182, 671
Kauffmann, G., White, S. D. M., & Guiderdoni, B. 1993, MNRAS, 264, 201
Kauffmann, G., et al. 2003, MNRAS, 346, 1055 (K03)
Kaviraj, S., Devriendt, J. E. G., Ferreras, I., & Yi, S. K. 2005a, MNRAS, 360, 60
Kaviraj, S., Ferreras, I., Yoon, S.-J., & Yi, S. K. 2005b, A&A, 439, 913
Khochfar, S., & Burkert, A. 2003, ApJ, 597, L117
Kinney, A. L., Calzetti, D., Bohlin, R. C., McQuade, K., Storchi-Bergmann, T., & Schmitt, H. R. 1996, ApJ, 467, 38
Knapp, G. R. 1999, in ASP Conf. Ser. 163, Star Formation in Early Type Galaxies, ed. P. Carral & J. Cepa (San Francisco: ASP), 119
Knapp, G. R., Guhathakurta, P., Kim, D.-W., & Jura, M. A. 1989, ApJS, 70, 329
Knapp, G. R., & Rupen, M. P. 1996, ApJ, 460, 271
Kong, X., Charlot, S., Brinchmann, J., & Fall, S. M. 2004, MNRAS, 349, 769
Larson, R. B. 1974, MNRAS, 166, 585
Martin, D. C., & the *GALEX* Team. 2005, ApJ, 619, L1
Morrissey, P., & the *GALEX* Team. 2005, ApJ, 619, L7
Peebles, P. J. E. 2002, in ASP Conf. Ser. 283, A New Era in Cosmology, ed. N. Metcalfe & T. Shanks (San Francisco: ASP), 351
Peng, E. W., Ford, H. C., & Freeman, K. C. 2004, ApJ, 602, 705
Press, W. H., & Schechter, P. 1974, ApJ, 187, 425
Pritchet, C. 1979, ApJ, 231, 354
Proctor, R. N., & Sansom, A. E. 2002, MNRAS, 333, 517
Rejkuba, M., Greggio, L., & Zoccali, M. 2004, A&A, 415, 915
Rejkuba, M., Minniti, D., Silva, D. R., & Bedding, T. R. 2001, A&A, 379, 781
Rich, R. M., et al. 2005, ApJ, 619, L107
Schawinski, K., et al. 2007, ApJS, 173, 512
Schiminovich, D., van Gorkom, J. H., van der Hulst, J. M., & Kasow, S. 1994, ApJ, 423, L101
Schmidt, M. 1959, ApJ, 129, 243
Schweizer, F., Miller, B. W., Whitmore, B. C., & Fall, S. M. 1996, AJ, 112, 1839
Scoville, N. Z., & Wilson, C. D. 2004, in ASP Conf. Ser. 322, The Formation and Evolution of Massive Young Star Clusters, ed. H. J. G. L. M. Lamers, L. J. Smith, & A. Nota (San Francisco: ASP), 245
Simien, F., & de Vaucouleurs, G. 1986, ApJ, 302, 564
Somerville, R. S., & Primack, J. R. 1999, MNRAS, 310, 1087
Stanford, S. A., Eisenhardt, P. R. M., & Dickinson, M. 1998, ApJ, 492, 461
Tantalo, R., & Chiosi, C. 2002, A&A, 388, 396
Thielemann, F.-K., Nomoto, K., & Hashimoto, M.-A. 1996, ApJ, 460, 408
Tinsley, B. M. 1980, Fundam. Cosm. Phys., 5, 287
Toomre, A. 1977, in Evolution of Galaxies and Stellar Populations, ed. B. M. Tinsley & R. B. Larson (New Haven: Yale Univ. Obs.), 401
Toomre, A., & Toomre, J. 1972, ApJ, 178, 623
Trager, S. C., Faber, S. M., Dressler, A., & Oemler, A. J. 1997, ApJ, 485, 92
Trager, S. C., Faber, S. M., Worthey, G., & González, J. J. 2000a, AJ, 119, 1645
———. 2000b, AJ, 120, 165
van den Hoek, L. B., & Groenewegen, M. A. T. 1997, A&AS, 123, 305
van Dokkum, P. G., & Franx, M. 2001, ApJ, 553, 90
van Dokkum, P. G., Franx, M., Fabricant, D., Illingworth, G. D., & Kelson, D. D. 2000, ApJ, 541, 95
van Dokkum, P. G., Franx, M., Fabricant, D., Kelson, D. D., & Illingworth, G. D. 1999, ApJ, 520, L95
Weiss, A., Peletier, R. F., & Matteucci, F. 1995, A&A, 296, 73
Wilcots, E. M., Hodge, P., Eskridge, P. B., Bertola, F., & Buson, L. 1990, ApJ, 364, 87
Yi, S., Demarque, P., & Oemler, A. J. 1997, ApJ, 486, 201
———. 1998, ApJ, 492, 480
Yi, S. K. 2003, ApJ, 582, 202
Yi, S. K., Peng, E., Ford, H., Kaviraj, S., & Yoon, S.-J. 2004, MNRAS, 349, 1493
Yi, S. K., Yoon, S.-J., Kaviraj, S., Deharveng, J.-M., & the *GALEX* Science Team. 2005, ApJ, 619, L111
Young, L. M. 2005, ApJ, 634, 258